Biophysical Journal Volume 96 January 2009 521–539

Phase Equilibria in DOPC/DPPC-d_{62}/Cholesterol Mixtures

James H. Davis,* Jesse James Clair, and Janos Juhasz
Department of Physics, University of Guelph, Guelph, Ontario, Canada

ABSTRACT There is broad interest in the question of fluid-fluid phase coexistence in membranes, in particular, whether evidence for liquid-disordered (l_d)-liquid-ordered (l_o) two-phase regions or membrane "rafts" can be found in natural membranes. In model membrane systems, such phase behavior is observed, and we have used deuterium nuclear magnetic resonance spectroscopy to map the phase boundaries of ternary mixtures containing 1,2-dioleoyl-*sn*-glycero-3-phosphocholine (DOPC), chain-perdeuterated 1,2-dipalmitoyl-*sn*-glycero-3-phosphocholine (DPPC-d_{62}), and cholesterol. For both this ternary model system and the binary DPPC-d_{62}/cholesterol sytem, we present clear evidence for l_d-l_o two-phase coexistence. We have selected sample compositions to focus on this region of fluid-fluid phase coexistence and to determine its temperature and composition ranges. The deuterium nuclear magnetic resonance spectra for compositions near the l_d-l_o phase boundary at high cholesterol concentrations show evidence of exchange broadening or critical fluctuations in composition, similar to that reported by Vist and Davis. There appears to be a line of critical compositions ranging from 48°C for a DOPC/DPPC-d_{62}/cholesterol composition of 0:75:25, to ~−8°C for the composition 57:14:29. At temperatures below this two-phase region, there is a region of three-phase coexistence (l_d-l_o-gel). These results are collected and presented in terms of a partial ternary phase diagram that is consistent with previously reported results of Vist and Davis.

INTRODUCTION

Plasma membranes generally contain a large variety of lipids differing in headgroup, chain length, and degree of chain unsaturation. In model systems, the interactions between cholesterol and phospholipid molecules strongly favor the partitioning of cholesterol into domains rich in long saturated chain lipids rather than into domains having predominantly unsaturated lipids. It seems plausible that domains rich in cholesterol and long-chain saturated lipids may exist at least transiently in plasma membranes (1–3). It is also possible that these domains may select among the different proteins found in the plasma membrane, forming membrane rafts where the cholesterol-rich phase has a significantly higher degree of molecular order than the bulk membrane. These coexisting domains are thought to correspond to the liquid-ordered (l_o) and liquid-disordered (l_d) phases found in phospholipid/cholesterol binary mixtures (4–6). Membrane rafts extracted from plasma membranes using various detergents contain a large proportion of long-chain saturated lipids and high concentrations of cholesterol. Model membranes having such lipid and cholesterol compositions are known to form the liquid-ordered phase; thus, it is strongly believed that membrane rafts, if they exist in vivo, will be in the l_o phase at physiological temperatures. Our own NMR experiments on detergent-extracted membrane rafts show that these particles are in the l_o phase. Proof of the existence of membrane rafts in vivo remains difficult. However, studies of model systems provide a means of investigating the properties of coexisting l_d and l_o phases.

That incorporation of cholesterol into model membranes induces the formation of domains of two types, differing in composition (i.e., it induces a lateral phase separation), was first reported for binary mixtures of 1,2-di-d_{31}-palmitoyl-*sn*-glycero-3-phosphocholine (DPPC-d_{62})/cholesterol (4,7,8). In these mixtures, the cholesterol-rich phase has become known as the l_o phase and the cholesterol-poor phase as the l_d phase (the more familiar L_α or "fluid" phase). The distinction between these two phases is based on their different compositions and on the large difference in molecular (hydrocarbon chain) order (4), a result of the well known "ordering" effect of cholesterol (4,9–12). The increased molecular order results in an increase in membrane hydrophobic thickness (13) and membrane rigidity (11,14–16). These two phases differ from the familiar "gel" solid-ordered (s_o) phase primarily through their high degree of molecular mobility. For example, both axial and lateral diffusion rates are much higher in the l_d and l_o phases than in the gel phase (4,5,17–22).

In deuterium (^{2}H) NMR, the quadrupolar splittings are proportional to the carbon-deuterium (C-D) bond order parameters, making it easy to distinguish between phases such as l_d and l_o on the basis of their very different quadrupolar splittings. However, if the domains in the l_d-l_o two-phase coexistence region in DPPC-d_{62}/cholesterol are very small, at the rates of phospholipid lateral diffusion characteristic of these two phases, the molecules effectively sample both environments on the ^{2}H NMR timescale. In such a case, rather than seeing distinct ^{2}H spectra for the two domains at temperatures and compositions within this two-phase region, an exchange averaged spectrum would be observed (4,6). On the other hand, as discussed previously (4,8,12,23–25), it is also possible that the compositions

Submitted April 5, 2008, and accepted for publication September 30, 2008.
*Correspondence: jhd@physics.uoguelph.ca
Editor: Thomas J. McIntosh.

0006-3495/09/01/0521/19 $2.00
doi: 10.1016/j.bpj.2008.09.042

showing l_d-l_o phase coexistence are so close to a critical mixing point that rapid fluctuations in composition lead to broadening of the spectra. The ^{2}H NMR spectra reported here at higher cholesterol concentrations (near 30 mol %) and at higher temperatures have shown evidence of one or both of these effects. Additional careful experimentation and analysis will be required to distinguish between these two phenomena.

Recently, fluorescence (26–40) and NMR (24,25,33,40–43) studies of ternary mixtures such as 1,2-dioleoyl-*sn*-glycero-3-phosphocholine (DOPC)/DPPC/cholesterol or 1-palmitoyl,2-oleoyl-*sn*-glycero-3-phosphocholine/sphingomyelin/cholesterol have found evidence for large, stable domains of coexisting l_o and l_d phases over wide temperature and composition ranges. The key requirement for such mixtures to phase-separate in this manner seems to be a strong differential interaction between cholesterol and the two lipids. The preference of cholesterol for saturated chain lipids results in the formation of a highly ordered, cholesterol-rich phase containing a large proportion of the saturated lipid and a much more disordered, cholesterol-poor phase with a correspondingly high concentration of unsaturated lipid. Fluorescence microscopy on giant unilamellar vesicles using dyes that partition preferentially into one phase or the other has shown that these domains are very large and persist indefinitely (although the domains may slowly aggregate, often forming two very large domains, one for each of the two coexisting phases) (28,31,34,38,39). Already a broad range of experimental and theoretical approaches have been used to begin to map the phase boundaries in these ternary mixtures, and the coexistence of l_o and l_d phases is well established by fluorescence, NMR, electron paramagnetic resonance (EPR), x-ray diffraction, and atomic force microscopy measurements (24,25,27–29,31,33–36,38,42,44–54).

There are limitations associated with each technique, so it is important to examine these systems from many different perspectives. Fluorescence microscopy requires that the domains be large to be visualized. Thus, fluorescence microscopy is unable to detect the l_d-l_o two-phase region in binary DPPC/cholesterol mixtures. This technique also requires the use of fluorescence-labeled probes, which have been shown to influence the phase behavior being observed (40). The method of preparing giant unilamellar vesicles may also result in a heterogeneous distribution of vesicle compositions, which makes an accurate description of phase equilibria difficult. EPR also requires the use of spin-labeled probes, but these are somewhat less perturbing than the fluorescence probes usually used. Nonetheless, EPR probes may differentially partition among the available phases, making quantitative analysis more difficult. EPR benefits from having a spectroscopic timescale much shorter than that of NMR (typically 10^{-9} s for EPR compared to 10^{-4} s for ^{2}H NMR). Thus, using EPR allows the observation of more short-lived states, where NMR would show only an average. ^{2}H NMR makes use of the relatively nonperturbing replacement of ^{1}H by ^{2}H, allowing straightforward quantitative analysis of even multicomponent spectra. Using lipids with perdeuterated chains results in a shift of the melting (gel-to-l_d) transition to lower temperatures by ~4°C (4,55). This effect must be taken into account in comparing a phase diagram determined by ^{2}H NMR of perdeuterated lipids with those determined by other techniques. The spectroscopic timescale of ^{2}H NMR is rather long, so exchange of molecules between small coexisting domains or local fluctuations in composition may lead to an averaging of the spectra. This effect is very pronounced in DPPC-d_{62}/cholesterol mixtures and, as described below, is observed at higher temperatures even in the ternary DOPC/DPPC-d_{62}/cholesterol mixtures discussed here.

In the analysis of the phase equilibria of multicomponent systems, tie-lines cross regions of two-phase coexistence in such a way that all compositions along a tie-line are simply varying proportions of the same two types of single-phase domains, having compositions given by the endpoints of the tie-lines. Tie-lines can be determined experimentally in a number of ways provided that one has at least two samples with compositions along the tie-line. Determining tie-line endpoints establishes the phase boundaries of the two-phase coexistence regions. Because they provide a quantitative measure of the amounts of the two phases, spectroscopic techniques such as ^{2}H NMR (4,33,56) and EPR (48) are particularly well suited to determination of tie-line endpoints.

The coexistence of l_d and gel phases is well established in a wide variety of two-component lipid or lipid/cholesterol mixtures. The large differences between the spectra (either ^{2}H NMR or EPR) in these two phases makes quantitative measurement of the amount of each phase straightforward. Since both the l_o and gel phases are characterized by similar degrees of molecular (chain) order, it is more difficult to establish and quantitate the coexistence of these two phases. As discussed above, the primary difference between the l_o and gel phases is in the timescale and symmetry of the molecular motions. Nonetheless, quantitative analysis of the spectra can still provide a clear description of this two-phase coexistence region (4,5).

In two-component systems, such as DPPC-d_{62}/cholesterol, one can see three phases in equilibrium at only a single temperature. Such a three-phase line was reported by Vist and Davis (4). In a three-component system, however, three phases can coexist over a broad temperature/composition range. Such a three-phase region should exist in the DOPC/DPPC-d_{62}/cholesterol mixtures considered here, but so far there is little direct evidence for three phases in equilibrium (de Almeida et al. (52) recently reported observing three coexisting phases, but in only one particular vesicle, and Veatch et al. (25) attempt to decompose the ^{2}H NMR spectra into three independent components in an effort to demonstrate three-phase coexistence).

Below, we describe our ^{2}H NMR investigations of the DOPC/DPPC-d_{62}/cholesterol ternary-phase diagram. We have focused on the composition range where fluorescence studies have identified regions of stable two-phase l_d-l_o coexistence (31). Our samples consist of mixtures of DOPC, chain perdeuterated DPPC-d_{62}, and cholesterol, and were studied over the temperature range from 0 to 50°C. We have also repeated one of the compositions previously studied by Vist and Davis (4), that with a DPPC-d_{62}/cholesterol ratio of 3:1, because the original files have been lost. We have found that, at that composition, there is a narrow range of temperatures (from 38 to 42°C) where the ^{2}H NMR spectra clearly show two-phase coexistence. Previously, two-phase coexistence in this binary mixture had to be inferred from the intermediate exchange averaging of the spectra (4).

In the next section we describe the samples, the method of preparation, and the methods of analysis (including spectral subtraction and moment analysis). We then present our experimental results and analyze them in terms of a partial temperature/composition phase diagram. Finally, we present suggestions for clarifying some of the unresolved issues which are raised here.

MATERIALS AND METHODS

Sample preparation

DOPC was obtained from Avanti Lipids (Alabaster, AL) and used without further purification. DPPC-d_{62} was synthesized using the procedure of Gupta et al. (57). Cholesterol was obtained from Sigma-Aldrich (St. Louis, MO) and twice recrystallized from ethanol before use. Stock solutions of DOPC (2.5 mg/mL), DPPC-d_{62} (2.5 mg/mL), and cholesterol (2.5 mg/mL) in ethanol were used to prepare a set of 18 samples with DOPC/DPPC-d_{62}/cholesterol molar proportions of 45:45:10, 24:56:20, 32:48:20, 40:40:20, 48:32:20, 56:24:20; 0:75:25, 15:60:25, 22.5:52.5:25, 30:45:25, 37.5:37.5:25, 45:30:25, 52.5:22.5:25; 21:49:30, 28:42:30, 35:35:30, 42:28:30, and 49:21:30. The appropriate volumes of stock solution for each sample were mixed in a small, round-bottomed flask and the solvent was removed by rotary evaporation. Residual ethanol was removed under vacuum overnight at room temperature. Ethanol was chosen as a solvent because of the similar solubility of all three components in ethanol (4,7). This minimizes the degree of separation of the three components under solvent evaporation, improving the homogeneity of the resultant three-component mixture.

It is common practice to mix lipids and cholesterol using chloroform. As reported by Vist (7) and Vist and Davis (4), the use of chloroform can result in significant sample heterogeneity upon rotovapping or freeze-drying, especially at higher cholesterol concentrations (58,59). To quantitate this effect we carefully prepared mixtures of DPPC and cholesterol for comparison, using either chloroform or ethanol. ^{1}H solution NMR (at 300 K) was used to quantitate the cholesterol/DPPC ratios by integrating several separate peaks arising from the two components. Specifically, these were the cholesterol methyl resonance at 0.74 ppm, the DPPC glycerol-c2 proton at 5.26 ppm, the cholesterol H-6 peak at 5.36 ppm, and the DPPC γ-$(CH_3)_3$ peak at 3.24 ppm, all chemical shifts measured with respect to the d_4-methanol methyl peak at 3.32 ppm (assignments of cholesterol peaks are from Muhr et al. (60)).

A mixture of ~75 mg DPPC and cholesterol, having nominally 31.65% cholesterol, was dissolved in ethanol and another mixture, having nominally 29.48% cholesterol, was dissolved in fresh, dry chloroform. The two mixtures were separately rotovapped to dryness in pear-shaped flasks and then placed under vacuum (in a lyophilizer) for at least 8 h to remove all residual solvent. Samples of the films, deposited on each of the two flasks by rotary evaporation, were taken from four different locations: 1), the very bottom (center) of the flask; 2), the thickest portion of the film (corresponding to the last location to be dried); 3), the very edge of the film (the thinnest part of the film); and 4), an area well separated from the other three areas. Each of these samples contained ~5 mg of DPPC/cholesterol mixture. If the two components of the mixture precipitate at the same rate during solvent evaporation, then all areas of the film will have the same nominal composition. If the two components partially phase-separate during evaporation, we will see a variation in composition. The resulting heterogeneity will persist during subsequent hydration.

Each of the four areas sampled from the two films were then redissolved in d_4-methanol for analysis by solution NMR. The samples extracted from the ethanol solution had compositions of 31.67 ± 0.05, 31.68 ± 0.05, 30.84 ± 0.2, and 30.80 ± 0.2% cholesterol. Those from chloroform had compositions of: 27.74 ± 0.3, 27.85 ± 0.3, 30.36 ± 0.4, and 29.60 ± 0.2% cholesterol. The average composition from ethanol is 31.25%, with a range of ±0.44%, whereas from chloroform we found an average composition of 28.89% and a range of ±1.31%. There is a threefold increase in the width of distribution of sample compositions when chloroform is used instead of ethanol. Although the small number of samples used, and their relatively large size, underestimate the full range of sample heterogeneity in each mixture, the results give a clear indication of the relative merits of these two solvents. The increased sample heterogeneity when chloroform is used will broaden the ^{2}H NMR spectra and the phase boundaries observed in such mixtures and affect the interpretation.

We also observed, in solution NMR experiments in d-chloroform, that if precautions are not taken to ensure the dryness of the chloroform, the ^{1}H NMR spectra show multiple environments for both cholesterol and DPPC. It is presumed that these arise from association of small amounts of water (initially in either the chloroform or the lipid) with the lipid and cholesterol, leading to formation of colloidal particles (or local microdomains) within the solution. In such a case, the problem discussed above is much more severe. A solvent such as ethanol, in which water is freely miscible, will perform much better than one with limited water solubility.

After all the ethanol was removed, the samples were hydrated at room temperature in a snap-cap centrifuge tube with 50 mM potassium phosphate buffer, pH 7.0, at a total dry lipid weight to buffer volume ratio of 4:3. The total amount of lipid (DOPC, DPPC-d_{62}, and cholesterol) was varied to provide ~20 mg of DPPC-d_{62} in each sample. The hydrated mixture was then carefully mixed by hand using a small glass stirring rod. During the mixing process, samples were routinely heated to 50°C to fluidize the mixture and speed the mixing process. After stirring, the sample was centrifuged back to the bottom of the snap-cap vial and the process was repeated until the sample was homogeneously hydrated. The mixture was then transferred to short 4-mm glass NMR tubes by gentle centrifugation. Samples were sealed using a small red rubber stopper and weighed before and after use. There was no evidence of any water loss in any of the samples over the time course of the experiments. Samples were also tested by ^{1}H solution NMR for any evidence of sample degradation (formation of lyso-PC). We were unable to detect any sign of lyso-PC in our samples, with an upper limit of 0.5%. At the beginning of the NMR experiments, each sample was first heated to at least 50°C, where spectra were taken to assess the homogeneity of the sample. Only then did we begin the temperature-dependence experiments. These were all performed by sequentially lowering the sample temperature in small steps to the point desired, taking a new spectrum at each temperature. For example, a spectrum is taken at 50°C, then the temperature is lowered to 48°C and another spectrum is taken, then the temperature is lowered to 46°C, etc. The NMR spectra in the fluid phase (see Figs. 3 and 4 for examples) are characteristic of a fluid l_d phase and are representative of all of the samples.

After completing the temperature-dependence experiment on several of the samples, and freezing the samples for storage, we put the samples back into the magnet to repeat a few measurements, adding a few new

temperatures. In doing so, we found that the lineshape had sharpened noticeably. Initially, we thought that the freeze-thaw cycle had caused this change, so we repeated the measurements we had made, and all subsequent samples were subjected to this single freeze-thaw cycle. Typically, a sample was stored 1–3 days at −20°C before doing the NMR experiments. (The first few samples had been stored for as long as 3 months at −20°C.) It turns out that lengthening of the lineshape is most pronounced for those samples with the longest exposure to the magnetic field and that in samples for which the NMR experiments took only 2–3 days there was no noticeable effect. It is likely that prolonged exposure to the strong magnetic field caused some slight orientation of some of the samples, resulting in slightly sharper 90° edges and weaker shoulders (61,62). We observed no significant difference in the quadrupolar splittings or in the phase behavior. Spectral subtractions performed on spectra obtained before the freeze-thaw cycle are consistent with those from spectra obtained after the freeze-thaw cycle.

In a separate series of experiments we prepared a series of mixtures of DOPC and DPPC-d_{62} in order to obtain the phase boundaries for this mixture (M. Boudreau, L. Schmidt, J. H. Ziani, and Davis, University of Gulph, personal communication, 2008). Samples were prepared as described above at DOPC/DPPC-d_{62} ratios: 1:19, 1:9, 3:7, 4:6, 5:5, 6:4 and 7:3. The preliminary results of this study have been incorporated into the phase diagram presented here.

^{2}H nuclear magnetic resonance

All NMR experiments were performed on a 500-MHz wide-bore Bruker (Milton, Ontario, Canada) Avance II spectrometer at a ^{2}H NMR frequency of 76.77 MHz. The quadrupolar echo sequence (55,63) consists of two 90° pulses, with the second pulse phase-shifted by 90° with respect to the first pulse. The pulses were 1.8 μs in length and were separated by an echo delay of 21 μs for all acquisitions. This relatively short echo delay time was used to minimize the effects of differential relaxation (since components characteristic of the three phases l_o, l_d, and gel (s_o) may have differing T_2s). The short 90° pulse length minimizes spectral distortion and loss of intensity of the broad deuterium NMR lineshapes characteristic of the liquid-ordered and gel phases (55,64). One cannot overemphasize the importance of short pulse lengths and short refocusing delays in ^{2}H NMR spectroscopy. Very serious systematic errors will be made if the pulse lengths are much longer than those used here. For moment analysis and spectral subtraction, these factors and the flatness of the baseline are absolutely crucial. Typically, a total of 4096 scans were acquired for each spectrum using a recycle delay of 3 s. Cyclops phase cycling was used to minimize receiver channel asymmetry (65,66) and to improve the spectrum baseline by minimizing artifacts occurring after the pulses (55,63,66). The time domain quadrupolar echo signal was symmetrized (postacquisition) about the echo maximum so that there was always a data point precisely at the echo maximum (corresponding to $t = 0$) (66,67). The data points before the top of the echo were discarded and the remaining points were Fourier transformed, producing a frequency domain spectrum with an optimally flat baseline.

Spectral subtractions

In two-component mixtures, tie-lines in two-phase coexistence regions are isotherms. If, at a given temperature, several sample compositions give two-component spectra showing the coexistence of two phases, these spectra consist of differing amounts of two subspectra (or endpoint spectra) characteristic of the two phases in equilibrium. These samples lie on a tie-line that crosses the two-phase region and terminates at the phase boundaries (endpoints). Linear decomposition of the composite spectra, by subtracting a fraction of one two-component spectrum from another, can yield the endpoint spectra. Analysis of the amounts of each spectrum that must be subtracted from another to yield an endpoint spectrum will give the endpoint compositions (4,12,56). To obtain accurate endpoints using such an analysis, it is crucial to have undistorted, unrelaxed spectra; otherwise, the relative fractions of the two components deduced by the subtraction process will be incorrect.

In three-component mixtures, tie-lines in two-phase coexistence regions also lie within the isothermal plane, but their direction within that plane bears no obvious relation to the composition axes and must be determined experimentally. Furthermore, as the temperature is varied, the direction of the tie-lines will also vary, reflecting the changing shape of the two-phase coexistence region with temperature. Even within the isothermal plane, the tie-lines within a two-phase region need not be parallel (though they cannot cross). For these reasons, it cannot be expected that any particular set of samples will lie on a tie-line for a broad range of temperatures. However, for small temperature ranges it is possible that a well chosen set of samples will lie approximately on the tie-lines, and that spectral subtraction techniques can be used to obtain the endpoint spectra and endpoint sample compositions. Even if two (or more) sample compositions do not lie precisely on a given tie-line it may still be possible to perform subtractions and approximately determine the endpoints. Inspection of the spectra (see below) allows one to determine whether the tie-line through a given sample lies above (e.g., at higher cholesterol concentration) or below a second sample composition. Thus, even if the tie-line doesn't pass directly through two or more samples, it provides valuable information that can be used in constructing the phase diagram.

If two or more sample compositions lie precisely on a tie-line, the accuracy of the spectral subtraction procedure is determined by the fidelity of the experimental spectra. Factors such as signal/noise ratio and differential relaxation among the component spectra lead to uncertainty in the determination of the endpoint spectra. The estimated uncertainty for the values of K and K' are a measure of our ability to tell whether we have subtracted too much or too little of a given spectrum from another. If the sample compositions are not precisely on a tie-line, the subtraction process itself is imperfect, which will lead to an increased systematic error in determining the endpoint spectra and, consequently, the endpoint compositions. This increased uncertainty shows up immediately as an increased difficulty in determining the values K and K' (see below) of one spectrum, which must be subtracted from another to obtain an endpoint spectrum characteristic of either of the one-phase regions at the boundary with the two-phase coexistence region. It is clear that if the spectra are not precisely on the same tie-line, but are close, then using them in subtractions will still provide useful estimates of the endpoint locations but that there will also be a significant systematic error that is difficult to determine quantitatively. To help deal with the subjective nature of the subtraction procedure, we performed two independent sets of pairwise subtractions (two different individuals) and took the average of the two determinations, adding the difference between them in quadrature to the estimated uncertainty.

Scaling, or interpolation, of one or both spectra so that the splittings of one or the other of the component spectra match more closely (25,37) may make it seem easier to subtract spectra, but it introduces another systematic error, since the spectra being subtracted do not contain the appropriate ''amount'' of each phase (since the distance from each spectrum to the two endpoints along its own tie-line must be unique). This will give incorrect values for the endpoint concentrations. Depending on how close the sample whose spectrum has been scaled is to the phase boundary, and the relative slopes of the tie-line and the phase boundary, the error introduced by this process can be substantial. In our view, it is better to use the spectra as they are, keeping in mind the potential systematic error due to the changes in tie-line slope with temperature.

For two spectra, S_A and S_B, from samples of compositions A and B within an l_d-l_o two-phase coexistence region, where both spectra lie on the same tie-line, the spectra can be decomposed as

$$S_A = f_A \times S_{l_d} + (1 - f_A) \times S_{l_o}; \quad (1)$$

$$S_B = f_B \times S_{l_d} + (1 - f_B) \times S_{l_o}, \quad (2)$$

where f_A and f_B are the fractions of samples A and B that are in the fluid or l_d phase. We can then easily form linear combinations (subtractions) that yield the two endpoint spectra

$$S_{l_d} = S_A^{'} - K \times S_B^{'}, \tag{3}$$

where S'_A and S'_B are the experimental spectra normalized to unit area, and assuming that S'_A has a larger l_d fraction than S'_B, and

$$S_{l_o} = S_B^{'} - K^{'} \times S_A^{'}. \tag{4}$$

The values of K and K' are used to determine the endpoint concentrations. As illustrated in Fig. 1, the position of a given sample composition along the tie-line and the lever rule are used to determine the amount of sample in each of the two coexisting phases, where

$$\alpha_A = \frac{\overline{\mathbf{X}_{l_o} - \mathbf{X}_A}}{\overline{\mathbf{X}_{l_o} - \mathbf{X}_{l_d}}} \tag{5}$$

is the amount of sample A that is in the l_d phase and

$$\alpha_B = \frac{\overline{\mathbf{X}_{l_o} - \mathbf{X}_B}}{\overline{\mathbf{X}_{l_o} - \mathbf{X}_{l_d}}} \tag{6}$$

is the amount of sample B in the l_d phase. The fractions are given by the ratios of the lengths of the line segments along the tie-line, as shown in Fig. 1. When these line segments are projected onto the composition axes, we see that the ratios of the composition differences can also be used to determine these fractions. Thus,

$$\alpha_A = \frac{x_{l_o} - x_A}{x_{l_o} - x_{l_d}} = \frac{y_{l_o} - y_A}{y_{l_o} - y_{l_d}} = \frac{z_{l_o} - z_A}{z_{l_o} - z_{l_d}}, \tag{7}$$

where $\mathbf{X}_A = [x_A, y_A, z_A]$, etc., and x_A is the molar concentration of DOPC, y_A is the molar concentration of DPPC-d_{62}, and z_A is the cholesterol concentration of sample A.

Of course, the decomposition of the ^{2}H NMR spectra into its component spectra is determined by the partitioning of the DPPC-d_{62} between the two phases. Thus, the component of the spectrum arising from the l_d phase in sample A at any given temperature depends not only on the amount of sample in the l_d phase but also on the concentration of DPPC-d_{62} in that phase:

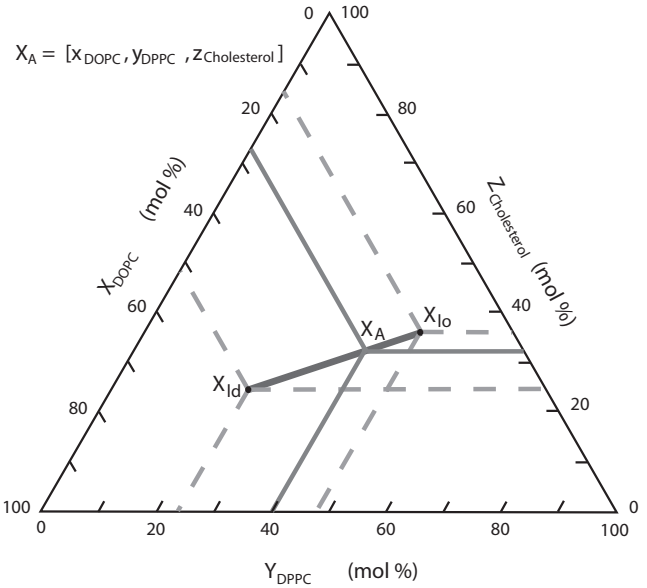

FIGURE 1 Example of the use of tie-lines to define end-point concentrations in two-phase coexistence regions. The intersections of the dashed lines with the composition axes give the compositions at the endpoints. The composition of any sample within the three-component triangle is given by the three mole fractions X_{DOPC}, $Y_{DPPC\text{-}d62}$, and $Z_{cholesterol}$.

$$f_A = \alpha_A \frac{y_{l_d}}{y_A}. \tag{8}$$

One could write analogous expressions for the other sample components. Inserting the expression for f_A into Eq. 1 and then solving Eqs. 3 and 4 for K and K',

$$K = \frac{\alpha_A y_B}{\alpha_B y_A} = \frac{\left(y_{l_o} - y_A\right) y_B}{\left(y_{l_o} - y_B\right) y_A} \tag{9}$$

and

$$K^{'} = \frac{(1 - \alpha_B) y_A}{(1 - \alpha_A) y_B} = \frac{\left(y_B - y_{l_d}\right) y_A}{\left(y_A - y_{l_d}\right) y_B}. \tag{10}$$

These expressions can be easily solved to give the endpoint DPPC-d_{62} concentrations:

$$y_{l_o} = \frac{(1 - K) y_A y_B}{y_B - K y_A} \tag{11}$$

and

$$y_{l_d} = \frac{\left(1 - K^{'}\right) y_A y_B}{y_A - K^{'} y_b} \tag{12}$$

Using the alternate forms for α_A and α_B (Eq. 7), we can solve for the endpoint concentrations of DOPC and cholesterol as well:

$$\begin{aligned} x_{l_o} &= \frac{K x_B y_A - x_A y_B}{K y_A - y_B} \\ x_{l_d} &= \frac{x_B y_A - K^{'} x_A y_B}{y_A - K^{'} y_B} \end{aligned}; \tag{13}$$

and

$$\begin{aligned} z_{l_o} &= \frac{K z_B y_A - z_A y_B}{K y_A - y_B} \\ z_{l_d} &= \frac{z_B y_A - K^{'} z_A y_B}{y_A - K^{'} y_B} \end{aligned}. \tag{14}$$

For a three-component system, it is possible for three phases to coexist over a finite composition and temperature range. At fixed temperature, the phase boundaries between this three-phase region and the neighboring two-phase region are two-phase lines. Since these two-phase lines connect endpoint one-phase regions on either side of the two-phase region, they are tie-lines (which must be straight lines). Thus, the three-phase region is bounded on three sides by straight lines and, consequently, is triangular in shape. The composition of any point within this three-phase region is given by the center-of-mass rule (68). Thus, an NMR spectrum at a temperature for which a sample has a composition lying within a three-phase region will consist of a superposition of three components, each one characteristic of one of the three phases. If one has spectra from three or more samples that all have compositions within the three-phase region at a single temperature, then, in principle, the amount of each of the three components can be determined by three-way spectral subtractions analogous to the preceding analysis of two-component spectra. Veatch et al. (40) use a related analysis method to find the vertices of the three-phase triangle at three temperatures. We will discuss their results in the concluding section of this article. We will not pursue this point further at this time, since it will not prove necessary for the analysis.

Moment analysis

The moments of the ^{2}H NMR spectra provide a powerful quantitative means of characterizing the degree of molecular order under the conditions of the experiment. The nth moment of the spectrum is defined, for symmetric ^{2}H NMR spectra, by

$$M_n = \frac{1}{A}\int_0^\infty \omega^n f(\omega)d\omega, \quad (15)$$

where $f(\omega)$ is the function describing the spectrum lineshape, ω is the angular frequency measured relative to the center of the spectrum (i.e., these are "central moments"), and

$$\mathrm{A} = \int_0^\infty f(\omega)d\omega$$

is the area of the spectrum (actually, half the area of the symmetric spectrum (55)). In calculating the moments from the experimental spectrum, we first determine an upper (lower) limit in frequency beyond which there is no spectral intensity (ω_∞) and then integrate first from 0 to $+\omega_\infty$, i.e., in the positive direction, then from 0 to $-\omega_\infty$, and add the magnitudes of the two results, giving the average over both halves of the symmetric spectrum.

If the molecules undergo rapid axially symmetric reorientation (i.e., rapid with respect to the ^{2}H NMR timescale), then the nth moment is proportional to the average of the nth power of the quadrupolar splitting (or of the nth power of the C-D bond order parameter S_{CD}) (55). The first moment, M_1, is then proportional to the average C-D bond order parameter, S_{CD}.

$$M_1 = \frac{4\pi}{3\sqrt{3}}\left(\frac{3e^2qQ}{4h}\right)\langle S_{CD}\rangle, \quad (16)$$

where $(3e^2qQ/4h) = 126$ kHz is the quadrupolar coupling constant for ^{2}H. Based on this, we have often used the parameter

$$\Delta_2 = \frac{M_2}{1.35M_1^2} - 1 = \frac{\langle S_{CD}^2\rangle - \langle S_{CD}\rangle^2}{\langle S_{CD}\rangle^2} \quad (17)$$

as a measure of the width of the distribution of quadrupolar splittings. For example, for a spectrum consisting of a single powder pattern (i.e., having a single quadrupolar splitting) the quantity Δ_2 would be 0 (55,56,69). This provides an easy way to detect coexisting phases that have different degrees of molecular order, since in such a case Δ_2 would differ significantly from 0. As we will see, a sudden increase in Δ_2 with temperature signals the beginning of a two-phase or three-phase coexistence region.

The C-D bond order parameters can be used to estimate the length of the lipid chains (70,71) through the relation

$$\langle L\rangle = 1.25\left\{\frac{N}{2} + \sum_i S_{CD}^i\right\}, \quad (18)$$

where N is the number of carbon-carbon bonds in the lipid chain and the sum is over all carbons (except the carbonyl) with C-D bond order parameters S_{CD}^i. In the all-*trans* configuration, all of the C-D bond order parameters are equal to 1/2. In that case, the chain length is just $L = 1.25N$. If it is assumed that the molecular volume of a lipid is constant, then changes in chain length can be related to changes in lipid cross-sectional area. Then the temperature coefficient of area expansion is given by

$$K_T = \frac{1}{A}\frac{dA}{dT} = -\frac{1.25N}{\langle L\rangle}\frac{d\langle S_{CD}\rangle}{dT}. \quad (19)$$

RESULTS AND DISCUSSION

Ternary mixtures of DOPC, DPPC-d_{62}, and cholesterol, when fully hydrated, can exist in at least three distinct phases as temperature and composition are varied. These are the liquid-disordered (l_d or fluid) phase, the liquid-ordered (l_o) phase, and the gel (s_o) phase. There are likely to be other phases formed at high cholesterol concentrations (we only examine samples of up to 30 mol % cholesterol), or at low hydration (our samples are fully hydrated). The ^{2}H NMR spectra of chain perdeuterated lipids in these three phases are quite different, allowing them to be used in determining phase boundaries and regions of phase coexistence. Fig. 2 shows spectra representative of these three phases. The spectrum in Fig. 2 *a* is typical of the model bilayer l_d phase. Each labeled chain position contributes its own powder pattern to the spectrum, with a quadrupolar splitting representative of the local carbon-deuterium bond order parameter, S_{CD}, at that position. The hydrocarbon chain flexibility gradient gives rise to the characteristic shape of the perdeuterated lipid spectrum (55). In the l_d phase, the lipid chains have a relatively high population of *gauche* conformers and *gauche-trans* isomerization is very rapid. The lipid molecules also undergo rapid axially symmetric reorientation about the bilayer normal (72,73) and rapid lateral diffusion (20). This high degree of mobility is consistent with the relatively loose packing of the chains within the bilayer, having a mean spacing of ~4.6 Å and with a relatively broad

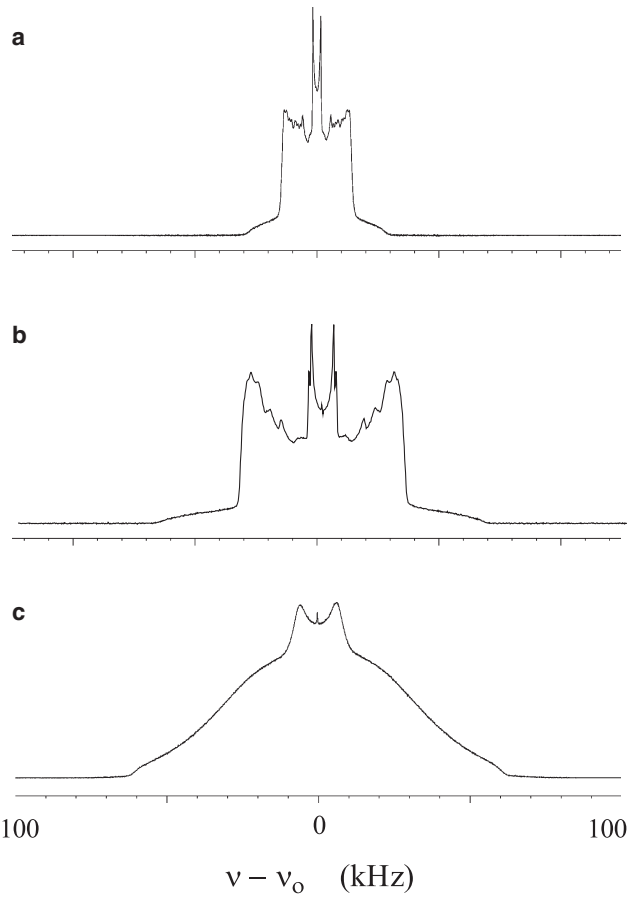

FIGURE 2 ^{2}H NMR spectra representative of three phases: (*a*) typical l_d phase of the DPPC-d_{62} bilayer above 37.75°C; (*b*) l_o phase at 36°C of DPPC-d_{62}/cholesterol at a molar ratio of 75:25; and (*c*) gel phase of DPPC-d_{62} below 37.75°C.

distribution of packing distances as shown by x-ray diffraction methods (42,74).

Fig. 2 *b* shows a spectrum representative of the l_o phase found at cholesterol concentrations >~20 mol % (this sample is for a binary mixture of 75 mol % DPPC-d_{62} and 25 mol % cholesterol). The overall shape of the spectrum is very similar to that of the l_d phase (Fig. 2 *a*). The principal differences between the spectra in the l_d and l_o phases are that the quadrupolar splittings for each position on the chain are considerably larger in the l_o phase than in the l_d phase and that the methyl groups on the two chains are inequivalent in the l_o phase (that of the *sn*-2 chain having a larger quadrupolar splitting than that of the *sn*-1 chain). The methyl group inequivalence is a useful indication of the presence of the l_o phase. In the l_o phase, the lipid chains have a reduced population of *gauche* conformers so that the chains are more extended, approaching the all-*trans* conformation at low temperatures (4). The molecules still undergo rapid axially symmetric reorientation about the bilayer normal, giving rise to the spectrum's axially symmetric lineshape (18,75). The rate of lateral diffusion is significantly reduced, however (20). Hydrocarbon chain packing in the l_o phase varies with the degree of chain order, being comparable to the l_d phase at higher temperatures but approaching that of the gel phase, 4.2 Å, at lower temperatures (42,76). Both Karmakar and Ragunathan (76) and Clarke et al. (42) report an increase in chain packing distance from 4.2 to >4.9 Å as cholesterol concentration is increased from 20 mol % (gel phase) to 60 mol % (l_o phase).

Fig. 2 *c* shows the spectrum found in the gel phase. The unusual bell shape arises from the intermediate-timescale motions characteristic of this phase. In the l_d and l_o phases, the molecules undergo rapid axially symmetric reorientation about the bilayer normal, giving rise to the axially symmetric powder-pattern lineshapes. In the gel phase, this motion is significantly slower, leading to the spectrum's characteristic shape (8,55,72,73,77). Since the shape of the gel phase ^{2}H NMR spectrum is strongly influenced by the timescale and nature of the motions in that phase, and since these motions themselves are sensitive to the temperature and composition of the sample, it is not surprising that the gel-phase spectrum changes significantly as the temperature and sample composition are changed. In addition, it is well known that the gel phase of pure phospholipid dispersions (such as DPPC/water) exhibits a transition from a rippled phase (P_β') to a nonrippled, tilted phase (L_β') near 28°C (74) and, at lower temperatures, a ''subtransition'' to a more tightly packed subgel phase (78,79). Thus, the phase behavior observed at low temperature may be somewhat more complicated than that presented here. When dealing with the low-temperature ''solid ordered'' (s_o) phase, we will simply refer to it as the gel phase, whether it is P_β', L_β', or some other highly ordered, solidlike hydrated lipid bilayer phase. A more complete phase diagram will have to address the boundaries between these different gel or solid phases.

Fig. 3 shows the variations that occur in the ^{2}H spectra for two different sample compositions as the temperature is lowered from 40 to 0°C. Fig. 3 *a* is for the DOPC/DPPC-d_{62}/cholesterol molar composition 40:40:20, whereas Fig. 3 *b* is for the composition 35:35:30. At 30°C and above, both samples appear to be in a well defined l_d phase. At 28°C, the sample with 20 mol % cholesterol is clearly in a two-phase, l_d-l_o coexistence region. The relative areas of the two components in the spectrum indicate that roughly equal amounts of DPPC-d_{62} are in each of the two phases.

At 28°C, the sample with 30 mol % cholesterol appears to be still in the l_d phase, although one can notice a slight broadening of the component powder patterns (this effect is noticeable even at higher temperatures for this sample). This broadening suggests that at this sample composition the system is showing evidence of intermediate-timescale phospholipid exchange between small domains of differing composition or, equivalently, of intermediate-timescale fluctuations in local sample composition (4,6,25). At 26°C, this effect becomes very clear and we see a spectrum at 30 mol % cholesterol characteristic of intermediate-timescale fluctuations. At this temperature and composition, we are close to

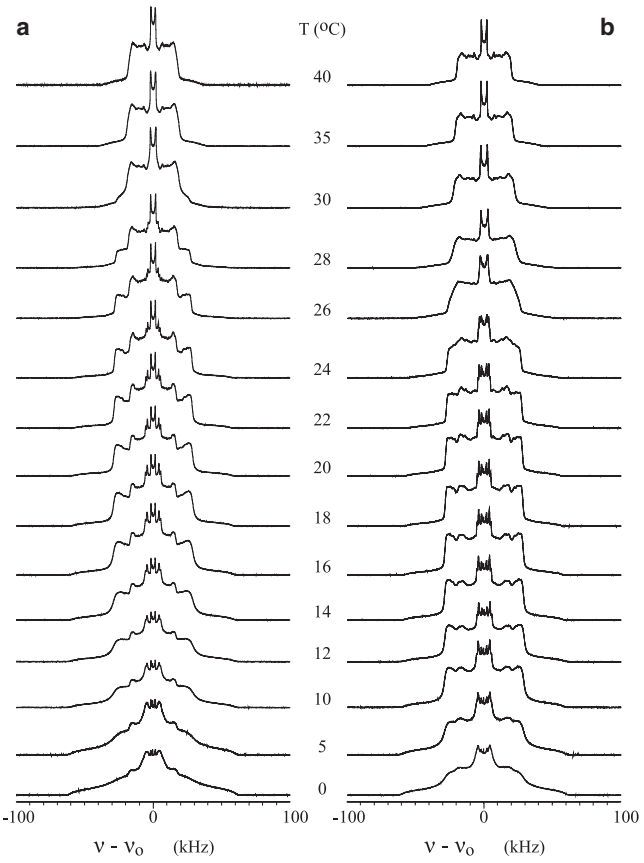

FIGURE 3 ^{2}H NMR spectra of DOPC/DPPC-d_{62}/cholesterol ternary mixtures at (*a*) 40:40:20 mol % and (*b*) 35:35:30 mol % versus temperature from 0 to 40°C. Notice the appearance and growth of the bell-shaped gel phase component at lower temperatures.

(probably slightly below) the boundary between the l_d phase and the two-phase, l_d-l_o coexistence region.

If the broadening is due to exchange of molecules between domains due to lateral diffusion (whether of cholesterol or phospholipid), it is easy to estimate the upper limit on domain size where this effect would be important. The relevant spectroscopic timescale is determined by the different quadrupolar splittings in the two types of domain. From Fig. 3, one can see that the l_d phase domains have a typical quadrupolar splitting of 32 kHz (the main 90° shoulder), whereas the l_o domains have a splitting of ~51 kHz. Half of this difference (which represents the difference in resonance frequency for lipids in the two domains) is $\Delta\nu \approx 6.5$ kHz. This defines the timescale as $\tau \approx 1/2\pi\Delta\nu \approx 25\ \mu$s. Using diffusion constants typical of the l_d and l_o phases (from 6×10^{-12} to 2×10^{-12} m^2/s (77)), from the relation $<r^2> = 4D\tau$, we estimate a maximum domain size of ~250 nm. Domains that are smaller than this will show evidence of exchange broadening, whereas domains significantly larger than this will not. This agrees well with the results of fluorescence microscopy, which is unable to detect domains for conditions under which ^{2}H NMR spectra show evidence of exchange broadening. Whether one wishes to explain the broadening of the spectra by diffusion between small domains or local fluctuations in composition (either of which leads to the molecules sampling different environments on the spectroscopic timescale), the effect is the same, a broadened spectrum and an enhanced T_{2e} relaxation rate (see below).

At 26°C, the sample with 20 mol % cholesterol (Fig. 3 *a*) is still within the two-phase coexistence region, but the proportion of l_o phase has increased at the expense of that of the l_d phase. This process continues for this sample as the temperature is lowered to 24°C, and the sample with 30 mol % cholesterol now also shows a clear two-phase, l_d-l_o coexistence. For this sample, the proportion of l_d phase is much smaller than for the sample with 20 mol % cholesterol, as expected, since the l_o phase is rich in cholesterol. As the temperature is lowered further, the amount of l_o phase continues to increase while that of the l_d phase decreases. The persistence of the narrowest methyl group component in the spectrum, indicative of the presence of the l_d phase, shows that some small fraction of the DPPC-d_{62} remains in the l_d phase even to quite low temperatures. Of course, DOPC remains in the fluid or l_d phase until ~−20°C (81,82), and some of the DPPC-d_{62} partitions into this phase (and we will see that some of the cholesterol is in this phase as well).

At 16°C and below, the spectra for the 20 mol % cholesterol sample begin to show evidence of a gel-phase component while still containing both l_d and l_o phase components. Thus, we may have entered a region of three-phase coexistence, l_d-l_o-gel. The sample with 30 mol % cholesterol stays in the two-phase region until ~10°C and below, where it also appears to enter a three-phase region. Below these temperatures, we continue to see possible three-phase coexistence, although it is becoming difficult to distinguish visually the presence of the l_o phase. We will see below that a moment analysis of the spectra can help to more accurately define the three-phase coexistence region.

It is also useful to inspect the variation in the ^{2}H NMR spectra with sample composition at a fixed temperature. For example, Fig. 4 shows the ^{2}H spectra at 26°C for nine

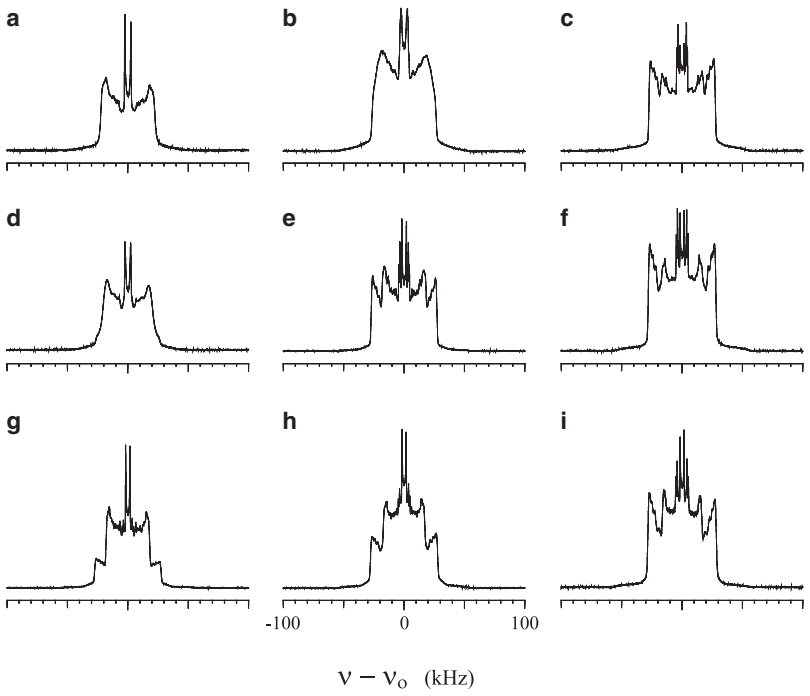

FIGURE 4 ^{2}H NMR spectra of nine different sample compositions at 26°C. DOPC/DPPC-d_{62}/cholesterol molar proportions: (*a*) 42:28:30, (*b*) 35:35:30, (*c*) 28:42:30, (*d*) 45:30:25, (*e*) 37.5:37.5:25, (*f*) 30:45:25, (*g*) 48:32:20, (*h*) 40:40:20, and (*i*) 32:48:20. The three spectra in the upper left corner (spectra *a*, *b*, and *d*) show evidence of either intermediate exchange between l_d and l_o domains or intermediate-timescale fluctuations in composition.

different sample compositions. The higher cholesterol concentrations are at the top of the figure, the higher DPPC-d_{62} concentrations are on the right, and the higher DOPC concentrations are on the left. At this temperature, the NMR spectra of the sample compositions shown in Fig. 4 that are on the diagonal (running from lower left to upper right) or below are well within the two-phase l_d-l_o coexistence region. The proportion of the l_o phase is larger for larger cholesterol and larger DPPC-d_{62} concentrations, whereas that of the l_d phase is larger for larger DOPC and smaller cholesterol concentrations.

The three spectra above this diagonal show evidence of intermediate-timescale exchange between small domains or fluctuations in local composition. It is clear that there is a phase boundary running close to the sample compositions that are one above the diagonal at this temperature. Fig. 5 shows the ^{2}H NMR spectra for the same set of samples at 22°C. Now, only the spectrum in the upper left corner of this array shows signs of exchange broadening; all of the others are clearly within the two-phase region. The phase boundary between the l_d phase and the two-phase, l_d-l_o coexistence region has moved toward higher DOPC and higher cholesterol concentrations. As one would expect, as the temperature is lowered and the DPPC-d_{62} concentration is increased, the proportion of l_o phase increases.

At 10°C, we see the gel phase forming for samples with a 20 mol % cholesterol concentration. It is particularly evident for the two spectra on the right of the bottom row in Fig. 6. At lower temperatures, the proportion of gel phase increases, and all samples eventually show at least some gel phase by 0°C. We will return to the question of three-phase coexistence below. In this fashion, examining changes in the ^{2}H NMR spectra as a function of temperature and sample composition, we can define the different phase-coexistence regions and the boundaries between them, allowing us to construct a partial phase diagram of this system.

As discussed above, if two or more samples have compositions that happen to lie on a tie-line within a two-phase coexistence region in the isothermal plane, it may be possible to perform pairwise subtractions to obtain spectra in which there is only a single component corresponding to one of the two coexisting phases. In general, it is not possible to predict the direction that a tie-line will take within the isothermal plane, and so it is more or less by chance if two or more samples happen to lie on a tie-line. The quadrupolar splittings observed in these ^{2}H NMR spectra are very sensitive to the cholesterol concentration (a consequence of the ordering effect of cholesterol). Comparison of the quadrupolar splittings of the component spectra coming from different sample compositions may reveal sets of spectra that have the same splittings. If the splittings of the component spectra match, then the domains that the component spectra represent must have similar compositions. In other words, if the only difference between the spectra of two samples of different composition (both within a two-phase coexistence region) at the same temperature is the relative amounts of the two spectral components, then these two sample compositions lie on a tie-line.

Fig. 7 shows three such two-component spectra at 26°C. The vertical dotted lines are drawn to indicate that each of the principal spectral features occur at the same frequency in each of the three spectra. For example, the very sharp

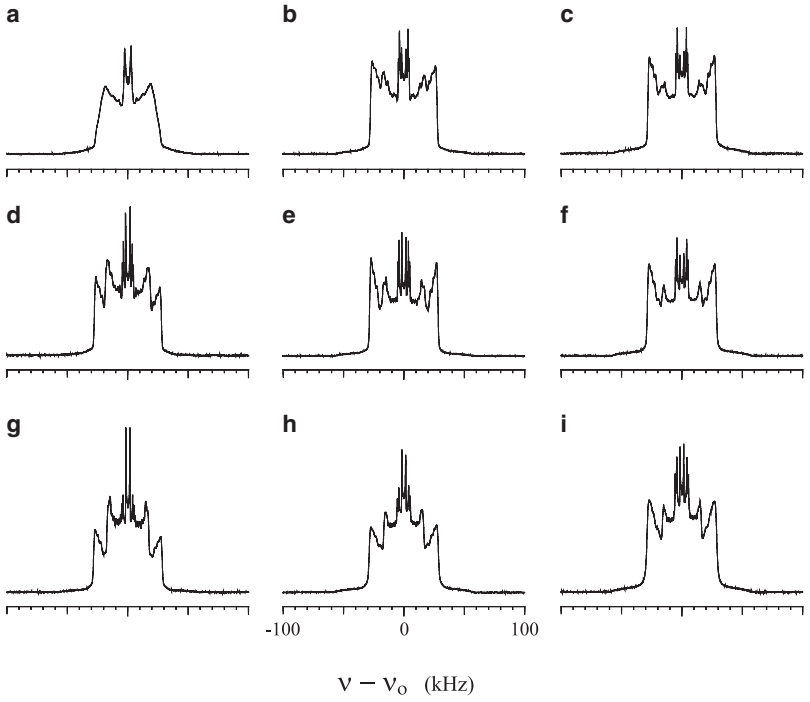

FIGURE 5 ^{2}H NMR spectra at 22°C of the same set of sample compositions as in Fig. 4. At this lower temperature, only spectrum *a*, in the upper left corner, shows evidence of intermediate-timescale averaging.

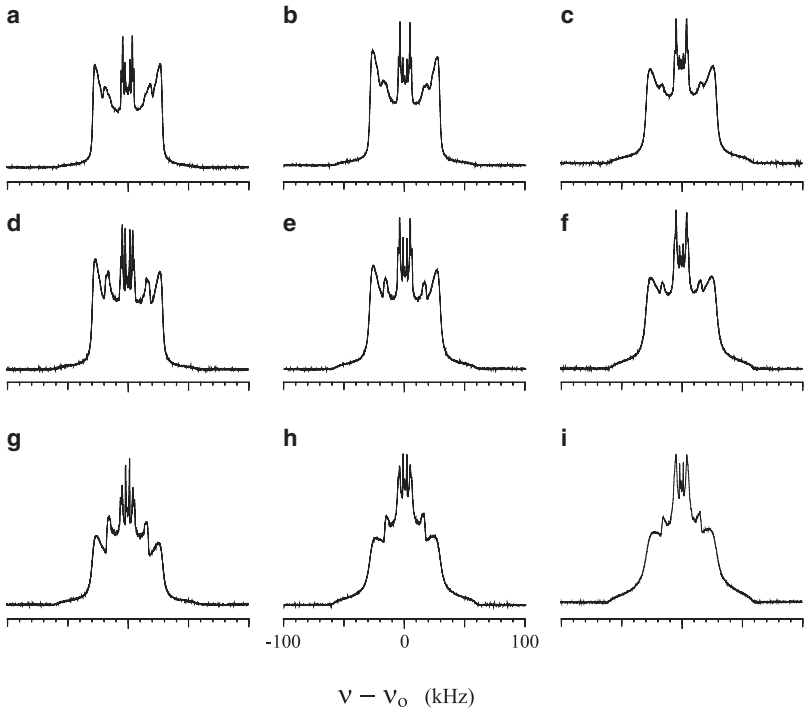

FIGURE 6 ^{2}H NMR spectra at 10°C of the same set of sample compositions as in Fig. 4. The spectra along and below the diagonal from bottom left to top right all show evidence of some gel-phase component while still exhibiting features indicative of the l_d and l_o phases. Notice especially the increasingly sloping shoulders and the growth of a broad component in the methyl-group region (near the center of the spectrum). Compare with the gel-phase spectrum of Fig. 2 *c*.

edges of the three methyl group powder patterns all occur at the same frequency, indicating that they all have the same quadrupolar splittings. Thus, these three sample compositions happen to lie very nearly along a single tie-line within the two-phase coexistence region. Any two of these spectra can be used to generate the endpoint spectra corresponding to either the boundary between the l_d-l_o two-phase region and the l_d phase or the boundary between the l_d-l_o two-phase region and the l_o phase.

When three samples lie along the same tie-line, we can perform three independent pairwise subtractions, as illustrated in Fig. 8 using spectra obtained at 28°C. We then use Eqs. 11–14 to determine the endpoint compositions. In Fig. 8 *a* (*upper*), the spectrum, S'_B, is for the sample with a DOPC/DPPC-d_{62}/cholesterol composition of 30:45:25 mol %, whereas in Fig. 8 *d*, the spectrum, S'_A, is for the sample with a composition of 40:40:20 mol %. Fig. 8 *b* shows the result of subtracting a fraction K' of S'_A from S'_B, whereas Fig. 8 *c* shows the result of subtracting a fraction K of spectrum S'_B from S'_A. The values of K and K' are used to determine the endpoint compositions. Although it is clear that the subtraction method yields spectra that are primarily representative of the two different phases, it is also evident that the subtraction process is not perfect. In particular, for this example, there is a small amount of l_o component still present in the l_d endpoint spectrum of Fig. 8 *c* (*arrow*). This is primarily a result of the fact that the sample compositions used for the subtraction are not precisely located on the same tie-line, although they are very close. Even so, the subtraction process works and can be used to give meaningful estimates of the endpoint compositions. At some temperatures, however, there will be significant systematic errors, since the same sample compositions will not lie on the same tie-lines at all temperatures. In fact, with our choice of sample compositions, the subtractions work better at higher temperatures, as the slope of the tie-lines more closely matches our compositions. As the temperature is lowered, the tie-line slopes change, and the systematic errors in subtraction increase accordingly.

Fig. 9 shows three different isothermal planes showing the estimated boundaries of the two- and three-phase regions for temperatures of 28°C (Fig. 9 *a*), 22°C (Fig. 9 *b*), and 18°C (Fig. 9 *c*). The endpoints from spectral subtractions are shown as solid right-pointing triangles (for the freeze-thawed samples) or open upward-pointing triangles (for the non-freeze-thawed samples) (l_d) and solid left-pointing triangles (for the freeze-thawed samples) or open downward-pointing triangles (for the non-freeze-thawed samples) (l_o). The error bars represent our estimated uncertainty in K and K' added in quadrature to the difference between two sets of independent determinations of the endpoint compositions starting from the same spectra. As indicated by the scatter in the points, the subtraction method works better at some temperatures than at others. The blue circles are points determined from moment analysis (Fig. 10) and partial ternary phase diagrams (see Fig. 12 below). The red triangle outlines the three-phase coexistence region.

Besides the determination of the boundary separating the l_d-l_o two-phase coexistence region from the l_d and l_o single-phase regions, the key step in constructing the phase diagram is determining the temperature dependence of the vertices of the three-phase triangle (*A*–*C*). The boundaries

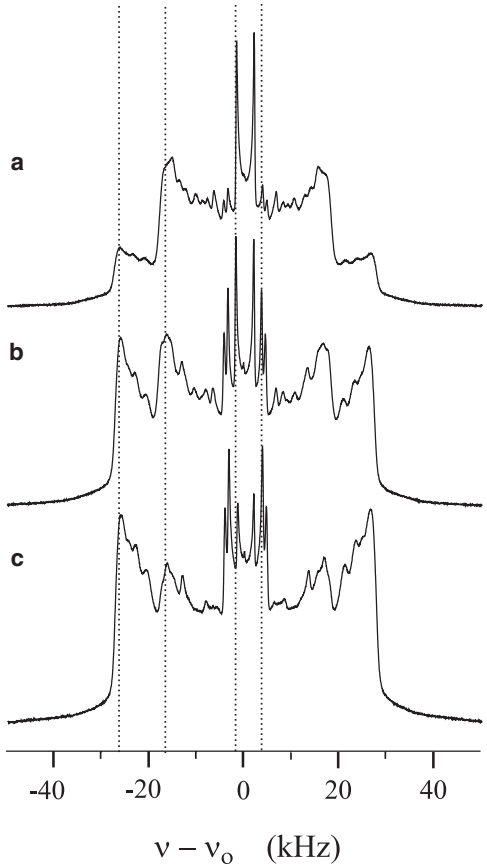

FIGURE 7 ^{2}H NMR spectra at 26°C of DOPC/DPPC-d_{62}/cholesterol molar proportions of (*a*) 48:32:20, (*b*) 37.5:37.5:25, and (*c*) 28:42:30. The vertical dotted lines are guides to the eye and indicate that each of the principal spectral features occur at nearly the same frequency in all three spectra. These three samples lie close to a common tie-line within the l_d-l_o two-phase coexistence region in the ternary phase diagram.

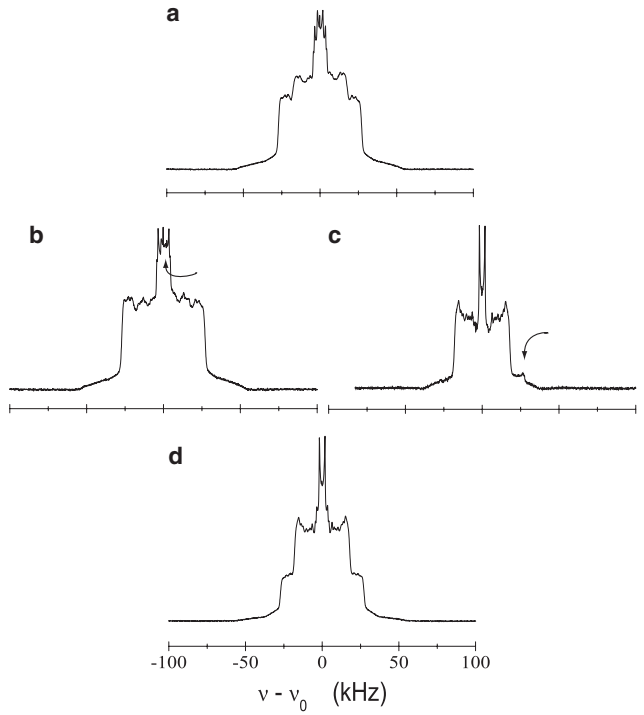

FIGURE 8 ^{2}H NMR difference spectroscopy at 28°C: (*a*) the spectrum S'_B of the sample with molar proportions 30:45:25 (normalized area); (*b*) the spectrum $S'_B - K'$ times the spectrum S'_A, with the area of the difference spectrum renormalized; (*c*) the spectrum $S'_A - K$ times that in S'_B, with the area renormalized; and (*d*) the spectrum S'_A of the sample with composition 40:40:20 (normalized area). The arrows indicate areas of the l_d phase difference spectrum that demonstrate the imperfect subtraction. It is these areas that we attempt to minimize in the subtraction process.

of the red triangles are formed by its interface with the l_d-l_o two-phase region on the left (line segment BC), the l_d-gel two-phase region below (line segment AB) and the l_o-gel two-phase region on the right (line segment AC). The gel phase boundaries are shown in green. Estimates of the critical composition at each of these temperatures are shown as magenta stars in this figure. A complete discussion of the determination of these phase boundaries can be found in the Conclusions section of this article.

Similar diagrams can be built at each temperature studied, giving us an overall picture of the temperature-composition phase diagram. One feature that can be expected for such diagrams is that as the temperature is increased, the three-phase triangle will approach the DPPC-d_{62}/cholesterol axis and will collapse into the three-phase line observed for DPPC-d_{62}/cholesterol mixtures at 37°C (4). In a similar way, as temperature is raised, the l_d-l_o two-phase coexistence region will approach and intersect the DPPC-d_{62}/cholesterol plane at 37°C and above. The ternary temperature/composition plot forms a triangular prism and the two-phase regions found within the body of the prism intersect with the planes forming its boundaries, thereby outlining two-phase coexistence regions in the DPPC-d_{62}/cholesterol and DOPC/DPPC-d_{62} two-component planes. The three-phase coexistence region that exists within the body of the prism can only intersect with the boundary plane in an isothermal line (which for this case occurs at 37°C in the DPPC-d_{62}/cholesterol plane and runs from ~7.5 to 20 mol % cholesterol). As temperature is decreased, the three-phase region eventually terminates within the body of the triangular prism and does not intersect either the DOPC/DPPC-d_{62} plane or the DOPC/cholesterol plane. Thus, the line of critical compositions also terminates at some critical temperature below which we cannot distinguish between l_d and l_o phases.

When a sample having a composition such that it will enter the l_d-l_o two-phase region is cooled through the two-phase region it will eventually enter the three-phase region that lies below. It does so by crossing line BC, below which some of the sample will begin to ''solidify'' into the gel phase. Thus, the surface traced out by the line BC as temperature is lowered defines the upper surface of the three-phase region. On continued cooling, the sample will eventually enter the l_o-gel two-phase coexistence region by crossing line AC, or, if it is close enough to the DOPC/DPPC-d_{62} plane, it may cross line AB, in which case it enters the

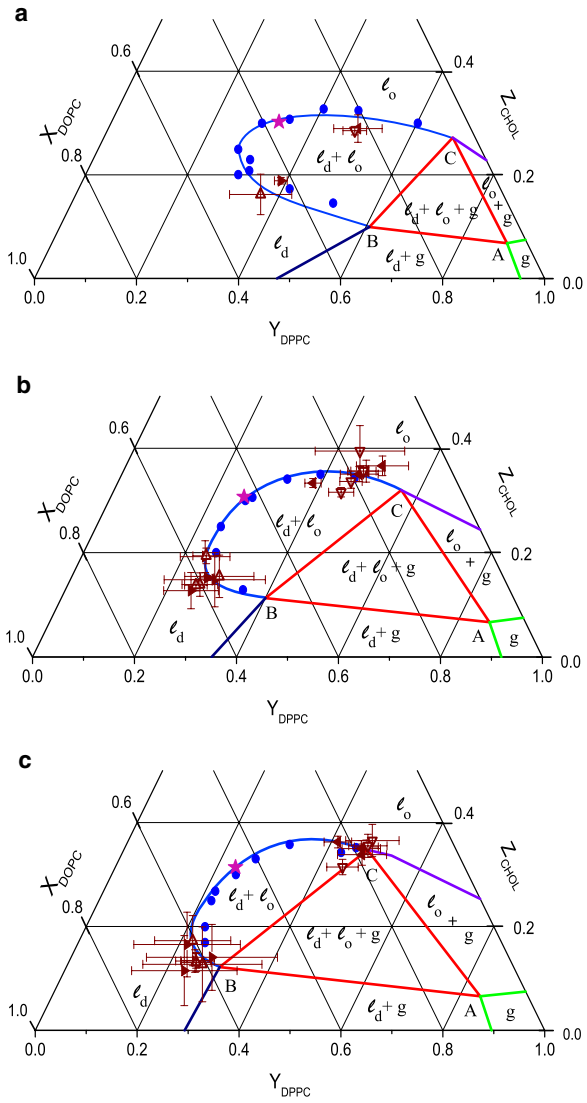

FIGURE 9 Isothermal planes of DOPC/DPPC-d_{62}/cholesterol ternary mixtures at (*a*) 28°C, (*b*) 22°C, and (*c*) 18°C. The different one-, two-, and three-phase regions are as labeled. The l_o phase endpoints obtained from spectral subtraction at each temperature are shown as left-pointing solid triangles (from the freeze-thawed samples) or downward-pointing open triangles (non-freeze-thawed samples), whereas the l_d phase endpoints are shown as right-pointing triangles (freeze-thawed samples) or upward-pointing open triangles (non-freeze-thawed samples). The error bars shown for the endpoints include estimated uncertainties of our imperfect subtractions that are largely due to the fact that our initial spectra do not lie exactly on the same tie-line (see text). The error bars also include the systematic differences between two independent determinations of the endpoints. The blue circles give the compositions where the fitted curves of Figs. 11 and 12 intersect the isothermal plane at that temperature. The estimated position of the critical composition at each temperature is shown by a magenta star.

l_d-gel two-phase region. Below the lower critical temperature, the sample will enter a ''fluid''-gel two-phase region before eventually solidifying into the gel phase.

The moments of the ^{2}H spectra provide a quantitative measure of the degree of molecular order, at least for phases exhibiting rapid axially symmetric motional averaging. Even in the absence of such rapid axial motion, the moments provide a measure of the degree of motional averaging. For now, we will concentrate on using the moments to study the temperature dependence of the distribution of quadrupolar splitting. In particular, M_1 gives the mean C-D bond order parameter, $\langle S_{CD}\rangle$, and Δ_2 gives the relative mean-squared width of the distribution of order parameters, $\langle(S_{CD} - \langle S_{CD}\rangle)^2\rangle/\langle S_{CD}\rangle^2$. Fig. 10 *a* shows the temperature dependence of $\langle S_{CD}\rangle$ for four samples with 25 mol % cholesterol. As the proportion of unsaturated chain lipid (DOPC) is increased, we see a reduction in the degree of chain order at all temperatures studied, but the overall variation of $\langle S_{CD}\rangle$ with temperature is similar for all four samples. Within the l_d, or fluid, phase, decreasing temperature not only results in an increase in the average chain order parameter, it also results in a narrowing of the distribution, Δ_2, as shown in Fig. 10 *b*. This reflects the fact that at lower temperatures the ''plateau'' in the order parameter distribution is becoming more pronounced as the chains are more tightly packed (the area/lipid is reduced as the temperature is decreased in the fluid phase).

As we cross the phase boundary from the l_d phase into the l_d-l_o two-phase coexistence region, we see an increase in Δ_2, reflecting the fact that the spectra now are a superposition of the narrower l_d phase spectrum and an l_o component that has much larger quadrupolar splittings. The temperature at which the change in Δ_2 begins can be used as a measure of the onset of the two-phase coexistence region. This onset correlates with the observation of an l_o phase component in the NMR spectra and/or the effect of intermediate timescale fluctuations on the spectrum. Lowering the temperature further within the two-phase coexistence region increases the amount of the l_o-phase spectral component and decreases that of the l_d phase. Thus, the width of the distribution of order parameters again begins to decrease, as shown in the figure. At sufficiently low temperatures, the parameter Δ_2 again begins to increase dramatically. This is characteristic of the onset of the gel phase and can be used to identify this phase boundary. In this case, the onset of the gel phase appears at slightly higher temperatures than is noticed simply by inspection of the spectra. Small amounts of gel phase component in the spectra may be masked by the large l_o-phase component, which has comparable quadrupolar splittings.

The gel-phase component in the ^{2}H spectrum is not characterized by rapid axially symmetric motion. Instead, it shows clear evidence of intermediate-timescale motions that lead to increased broadening of the quadrupolar doublets. This shows up as an increase in the width of the distribution of quadrupolar splittings. Although the dramatic increase in Δ_2 that occurs at low temperatures is caused by the appearance of the gel phase, it is not immediately clear whether this is proof of the coexistence of three phases, l_d, l_o, and gel. Furthermore, the behavior below the three-phase region remains unclear, and careful consideration of the

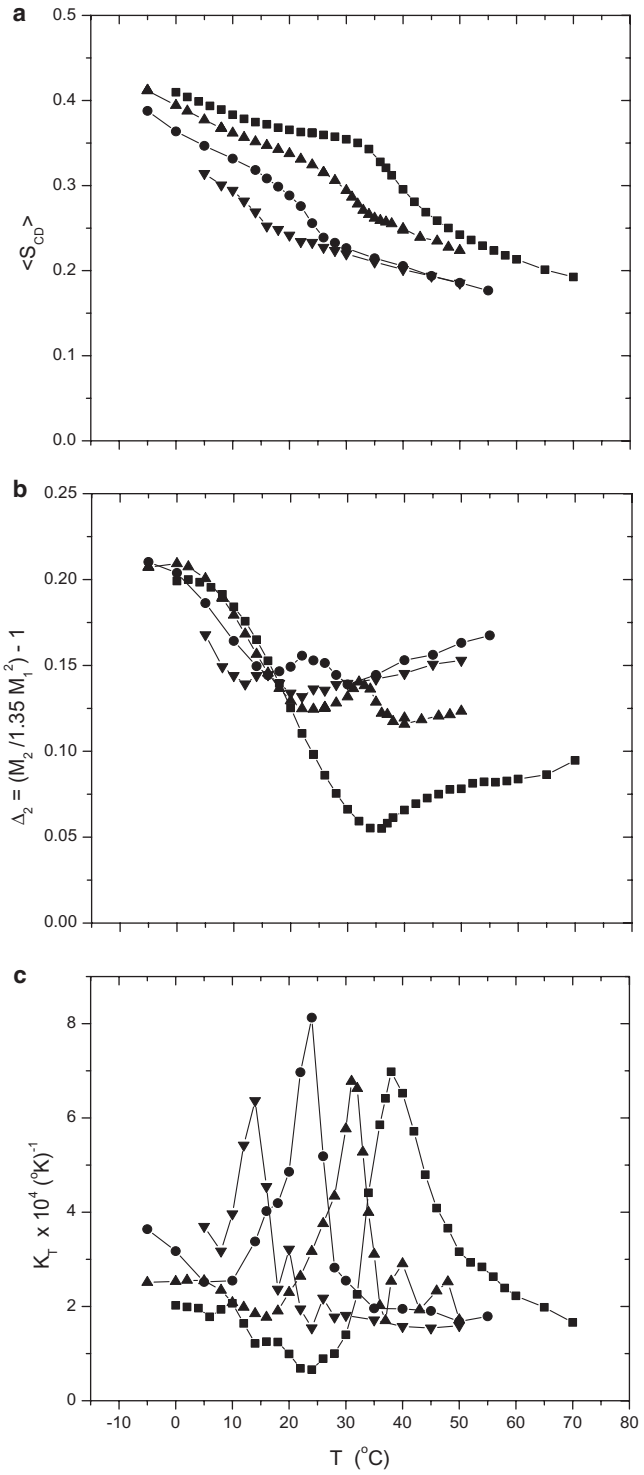

FIGURE 10 Temperature dependence of quantities derived from the moment analysis of the spectra for samples of 25 mol % cholesterol. (*a*) The average DPPC-d_{62} chain C-D bond order parameter, $\langle S_{CD}\rangle$. (*b*) The mean-squared width of the distribution of quadrupolar splittings, Δ_2. (*c*) The lipid chain thermal coefficient of area expansion, K_T. Samples were of molar proportions 0:75:25 (*squares*), 22.5:52.5:25 (*upward-pointing triangles*) 37.5:37.5:25 (*circles*), and 52.5:22.5:25 (*downward-pointing triangles*).

different types of ''gel'' phase will be needed to complete this part of the phase diagram.

The distribution of C-D bond order parameters is determined by the fluctuations in phospholipid chain bond orientations at different positions along the chain. The degree to which these fluctuations occur is determined by the packing of the chains within the membrane. The average length of the lipid chain is proportional to the average C-D bond order parameter (cf., Eq. 18). Assuming that the molecular volume is constant allows us to relate the changes in $\langle S_{CD}\rangle$ to changes in the cross-sectional area/lipid. The thermal coefficient of area expansion for these same four samples (having 25 mol % cholesterol) is shown as a function of temperature in Fig. 10 *c*. This provides an even more sensitive measure of the onset of the l_d-l_o two-phase coexistence region. The broad maxima in this coefficient occur over the temperature range where there is l_d-l_o two-phase coexistence. The area expansion coefficient is related to the lateral compressibility (83–86) and to the fluctuations in the chain order parameters. These properties will be influenced by any density fluctuations occurring near a critical point, so their measurement is a valuable tool for probing the nature of these fluctuations. Unfortunately, the width of the distribution of order parameters for our perdeuterated lipids is dominated by the variation of S_{CD} along the chain, so we cannot extract the area compressibility directly. Studies of the fluctuations of the C-D bond order parameter for specifically ^{2}H-labeled lipids could be more directly interpreted in terms of the area compressibility.

CONCLUSIONS

The sample compositions used in this study were chosen to cover the region of two-phase l_d-l_o phase coexistence to quantify its extent. Without having data over a far broader range of compositions we will need to make a few assumptions and simplifications to construct an approximate partial phase diagram for the DOPC/DPPC-d_{62}/cholesterol system.

First, we will incorporate the data of Vist and Davis (4) for the DPPC-d_{62}/cholesterol plane. In doing so, we have reanalyzed the original results and will close the l_d-l_o two-phase region at a DPPC-d_{62}/cholesterol mole ratio of 75:25 at 48°C. This point will be taken to be the upper critical temperature and one end of a line of critical compositions.

Second, we will include the preliminary results of an independent study of the phase equilibria of DOPC/DPPC-d_{62} mixtures (M. Boudreau, L. Schmidt, J.H. Ziani, and Davis, University of Guelph, personal communication, 2008) to define the phase boundaries in the DOPC/DPPC-d_{62} plane. We have fit their results for DOPC/DPPC-d_{62} to simple cubic polynomials to allow us to define the fluidus and solidus boundaries in this plane. Our ternary phase diagram will be required to agree with each of these two-component phase diagrams.

Next, in the absence of any definitive data for DOPC/cholesterol mixtures, we assume that above 0°C, DOPC

and cholesterol are miscible and that there are no phase boundaries in the DOPC/cholesterol plane below ~35 mol % cholesterol.

The boundaries for the l_d-l_o two-phase region are determined by moment analysis, spectral subtraction (where possible), and inspection of the spectra. This gives us limits for the range of this two-phase region both laterally (in composition) and vertically (in temperature).

As mentioned earlier, we will continue to ignore the differences between the P_β', L_β', L_β, and subgel phases and consider them all as the ''gel'' phase. Attempting to include these phases in the description is not possible at this time.

Although the ^{2}H NMR spectra of DOPC/DPPC-d_{62}/cholesterol samples having the range of compositions studied here and elsewhere (25,33) are certainly suggestive of three-phase coexistence over part of the temperature range, it remains difficult to identify unambiguously three components in the spectra of these perdeuterated lipids. Although it is possible in principle to perform three-way decomposition of the spectra within the three-phase region, the large uncertainty associated with even two-way subtractions has prevented us from attempting this type of analysis (although an attempt at a similar sort of analysis has been reported by Veatch et al. (25), see below). The moment analysis discussed above supports our interpretation of three-phase coexistence and provides a means of identifying the range of temperature over which it occurs. In addition, the rules for constructing phase diagrams in such systems lead us to predict a significant region of three-phase coexistence that intersects the DPPC-d_{62}/cholesterol plane at the three-phase line at 37°C reported by Vist and Davis (4).

At any given sample composition, cooling through the l_d-l_o two-phase region into the three-phase region that lies below it, we pass the interface between the three-phase and two-phase regions at line segment BC. The surface that this line segment traces out as temperature is varied forms the bottom surface of the two-phase region and the upper surface of the three-phase region. Thus, we may identify from the spectra and their moments the temperature at which we pass this interface. In a similar way, the surface traced out by line segment AC forms the bottom (lower-temperature) surface of the three-phase region and the upper surface of the two-phase l_o-gel coexistence region that lies below. However, this part of the phase diagram remains unclear. One complicating factor is that below ~+8°C, DPPC-d_{62} and DOPC/DPPC-d_{62} mixtures undergo a kinetically slow phase transition into a subgel phase, making the acquisition of equilibrium spectra very difficult. Since the kinetics of this phase transition depend on composition, it is difficult to be certain that all samples have adequately equilibrated below +8°C, and the large changes in lineshape that occur in the subgel phase, among other things, make spectral subtractions unreliable. In any case, analysis of our spectra and their moments shows that the three-phase region collapses into a two-phase phase line at the temperature corresponding to the other end of the line of critical concentrations, where line segment BC (Fig. 9) is reduced to a point and line segments AB and AC coincide. From our analysis, this occurs at ~−8°C.

At any given temperature (between −8 and $+48^\circ C$), the critical concentration will occur when the compositions of the l_d and l_o phases become equal, i.e., when the tie-line joining them is reduced to a point. At 48°C, this occurs at a composition of roughly $\vec{X}_{C_f} = [0, 0.75, 0.25]$ and at −8°C it occurs roughly at $\vec{X}_{C_i} = [0.57, 0.14, 0.29]$. These are the endpoints of the line of critical concentrations. Beyond these critical compositions at any given temperature the l_d and l_o phases are indistinguishable.

In the absence of detailed data concerning the limits of two-phase l_d-gel and l_o-gel coexistence regions within the body of the ternary triangular prism, we will simply join the vertices of our three-phase triangles (at any given temperature) to the corresponding phase boundaries on the DPPC-d_{62}/cholesterol and DOPC/DPPC-d_{62} planes with straight line segments. We do have one sample, with molar proportions 45:45:10, which lies between the l_d-l_o coexistence region and the DOPC/DPPC-d_{62} plane. At this composition, there is no evidence for an l_o phase, but the sample does display a broad l_d-gel two-phase coexistence region (see Fig. 11 *b*). Later experimental data can be used to define the curvature of these two-phase surfaces more accurately.

The curves traced out by the vertices of the three-phase region begin in the DPPC-d_{62}/cholesterol plane at 37°C (4). The curve corresponding to vertex A begins at ~7.5 mol % cholesterol, the lower limit of cholesterol concentration on the three-phase line of Vist and Davis (4). The curve corresponding to vertex B begins at the DPPC-d_{62}/cholesterol eutectic point, at ~9 mol % cholesterol, and the curve corresponding to vertex C begins at ~20 mol % cholesterol, the upper limit on cholesterol concentration of the three-phase line. For temperatures between ~50 and 0°C we are able to estimate the extent of the l_d-l_o two-phase region, either through spectral subtraction or by inspection of the spectra, and to determine the location of vertices B and C. We further estimate that the three-phase region, and therefore the line of critical compositions, must persist till ~−8°C, because we observe an l_d component to the spectra of several samples down to −7°C. A least-squares fit is performed to determine the path followed by curves B and C using the starting points above and these estimates as a function of temperature. The curves B and C meet at the lower critical temperature, −8°C.

The curve traced out by vertex A is much more difficult to determine experimentally using the data available to us. We have only been able to assume that it tracks the lower temperature limit (the solidus curve) for the DOPC/DPPC-d_{62} mixtures, and that it terminates at the chain-melting transition for pure DOPC/water at ~−20°C. Thus, there is a great deal of uncertainty in the variation of this vertex with temperature. Careful measurement of the extent of l_o-gel and l_d-gel

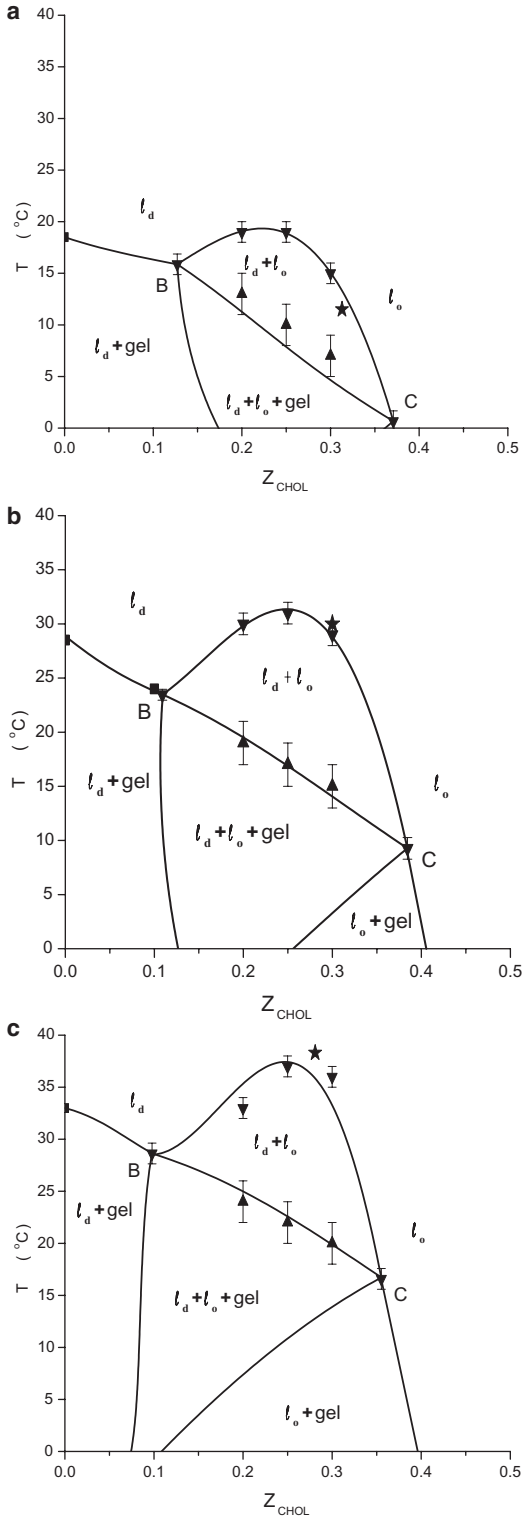

FIGURE 11 Titration diagrams showing the phase boundaries at constant ratios of DOPC/DPPC-d_{62} as cholesterol concentration is varied. DOPC/DPPC-d_{62} ratios were 7:3 (*a*), 1:1 (*b*), and 3:7 (*c*). The square data points give the onset temperatures for l_d-gel phase coexistence. The downward-pointing triangles show the upper limit of the l_d-l_o two-phase coexistence region determined from the ^{2}H NMR spectra, either from direct observation of two distinct components in the spectra, from the appearance of intermediate-timescale averaging effects in the spectra, or from moment analysis. The upward-pointing triangles show the boundary between the two-phase region above and the l_d-l_o-gel three-phase coexistence region below. These points were determined from the appearance of a gel-phase component in the spectrum and/or from moment analysis. The other phase boundaries show the locus of points at the intersection of the phase boundaries from the phase diagram in Fig. 12, with the plane at a given DOPC/DPPC-d_{62} ratio. The estimated positions of the critical composition are shown by stars.

two-phase coexistence is required before we can accurately determine the location of this phase boundary. We do know, however, that the vertices of the three-phase region must move with decreasing temperature in a way consistent with the rules for the construction of ternary phase diagrams.

To help define the upper surface of the l_d-l_o two-phase region we used the B and C vertex values corresponding to each of the five different DOPC/DPPC-d_{62} ratios (3:7, 2:3, 1:1, 3:2, and 7:3) used in the cholesterol titration experiments and the upper temperature limits estimated at each cholesterol concentration used (20, 25, and 30 mol %). We fit each set of points at fixed DOPC/DPPC-d_{62} ratio to a cubic polynomial to obtain a smooth curve. The results of these fits are shown in Fig. 11, with points B and C labeled on each curve. We also performed fits at fixed cholesterol concentration to obtain another set of boundary curves. These curves are all shown in dark blue on the phase diagram in Fig. 12. A similar analysis was performed at fixed temperature, starting again with the values of B and C at that temperature and including the estimates of the lateral (composition) limits of the l_d-l_o two-phase region (cf. Fig. 9). All of these results were then combined to yield the partial phase diagram shown in Fig. 12. In this figure, the three-phase region is outlined by the red triangles and the dark blue boundary curves tracing out the temperature variation of vertices B and C. The l_d-l_o two-phase region is outlined above by the dark blue curves determined from the analysis of Figs. 9 and 11 and below by the line segments BC of the three-phase triangles. The estimated extent of the gel phase is outlined by green curves in the DOPC/DPPC-d_{62} plane, the DPPC-d_{62}/cholesterol plane, and the curve for vertex A of the three-phase triangle. The DOPC/DPPC-d_{62} fluidus is shown in light blue. The results of Vist and Davis (4) are included on the DPPC-d_{62}/cholesterol plane along with our reanalysis of the extent of their l_d-l_o two-phase coexistence region. The estimated line of critical compositions is shown in magenta in Fig. 12. The upper and lower temperature limits of the l_d-l_o two-phase region are shown as black diamonds.

Veatch et al. (25) have published a phase diagram for the same three-component system. We are in broad agreement regarding the lateral extent of the l_d-l_o two-phase region below ~30°C, and these data agree with the fluorescence work as well (24,31). As previously mentioned, these authors perform a three-way decomposition of the ^{2}H NMR spectra in the three-phase region and determine the vertices of the three-phase triangles at three temperatures: 20, 15,

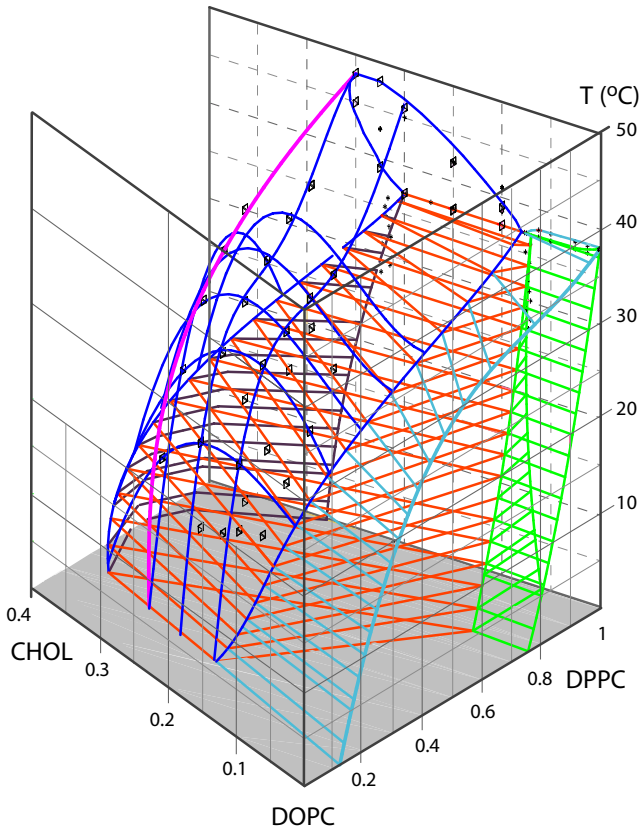

FIGURE 12 Approximate partial phase diagram for the DOPC/DPPC-d_{62}/cholesterol ternary system. The data on the DPPC-d_{62}/cholesterol face (at the back of the figure) are from Vist and Davis (4), except that the boundary with the two-phase l_d-l_o region has now been closed. The black squares show the upper and lower limits of the l_d-l_o two-phase region, as shown in Fig. 11. The dark blue curves are fits to the data described in Figs. 9 and 11 and show the upper surface of the l_d-l_o two-phase region. The red triangles represent the isothermal-plane cross sections of the three-phase coexistence region. The green lines indicate the approximate limits of the gel-phase region and the light blue lines mark the boundaries between the l_d phase and the l_d-gel two-phase coexistence region. The magenta line gives the approximate location of the line of critical compositions, running from ~−8 to 48°C.

and 10°C (see the supplementary material provided in the work by Veatch et al. (25)). There are, unfortunately, some inconsistencies in the supplementary data provided with that article, so that it is difficult to associate some of the spectra with the sample compositions used (see Veatch et al. (25), Supplementary Fig. 6). Nonetheless, despite these inconsistencies, the authors have demonstrated the potential of using spectral subtraction approaches in three-phase regions.

The principal difference between the phase diagram presented here and that presented by Veatch et al. (25) lies above 30°C. Eight of our samples (those having the highest cholesterol and DPPC-d_{62} concentrations) show evidence of two-phase coexistence above 30°C. Fig. 13 shows an expansion of the methyl group region for two of these samples. Fig. 13 *a* shows the methyl group spectrum for the sample with molar proportions 0:75:25 (25 mol % cholesterol in DPPC-d_{62}) for temperatures from 36 to 46°C. Between 38 and 42°C, we see clear evidence for two-phase coexistence, even for this two-component mixture, as predicted by Vist and Davis (4). As shown in the figure, the range of temperatures over which one observes two phases in coexistence is very narrow. In addition, the difference between the splittings in the two phases is very small compared to the difference observed in the three-component systems (see Fig. 13 *b*). Presumably, the large proportion of DOPC in the l_d domains in the three-component mixtures leads to the much smaller splittings. If the signal/noise ratio is poor or the line widths a little larger than those shown here, the two-phase coexistence in the two-component system may be difficult to observe, which may explain why it has not been noticed previously. Fig. 13 *b* shows spectra from the sample with molar proportions 21:49:30. Here, we see clear l_d-l_o two-phase coexistence above 30°C, with resolved resonances up to 33°C and evidence of intermediate-timescale fluctuations or exchange at 35°C and above. Furthermore, while Veatch et al. (25) choose to ignore the results of Vist and Davis (4) and Scheldt et al. (87), we have explicitly included the results of Vist and Davis in our ternary phase diagram.

Veatch et al. (25) also investigate the influence of possible critical fluctuations in composition on the decay of the quadrupolar echo, described by the relaxation time T_{2e}. Such measurements will be important in determining the nature of the intermediate-timescale averaging occurring at the high cholesterol limit of the l_d-l_o two-phase coexistence region (near the line of critical compositions). However, contrary to the claims of Veatch et al. (25), comparison of the quadrupolar echo relaxation rate to the linewidth of ^{2}H MAS spectra (see Fig. 4 *e* in Veatch et al. (25) says nothing about any inhomogeneous distribution of quadrupolar splittings that may exist. The quadrupolar echo sequence (63) refocuses the static quadrupolar interaction, and the decay of the echo itself, characterized by T_{2e}, is the result of fluctuations in the quadrupolar interaction that occur during the time interval between the first pulse and the formation of the echo. Magic-angle spinning removes the quadrupolar splittings, as well as any inhomogeneous distribution of those splittings that may be caused by sample heterogeneity. That T_{2e} should be able to account for the ^{2}H MAS line width is expected.

^{2}H NMR powder-pattern spectra are, by definition, strongly inhomogeneously broadened by the residual quadrupolar interaction. This gives rise to the observed quadrupolar splittings and the powder-pattern lineshape. Another source of ''inhomogeneous'' broadening is the distribution of quadrupolar splittings along the chains. Hole-burning experiments (88) demonstrated that the DPPC ^{2}H powder pattern was inhomogeneously broadened but that lateral diffusion would provide a mechanism (albeit slow) for filling in the hole burned in the spectrum. This effect explained why spin-lattice relaxation, T_1, appears to be nearly uniform over the entire powder-pattern lineshape, but transverse spin relaxation, T_{2e}, is found to depend on orientation. It is also

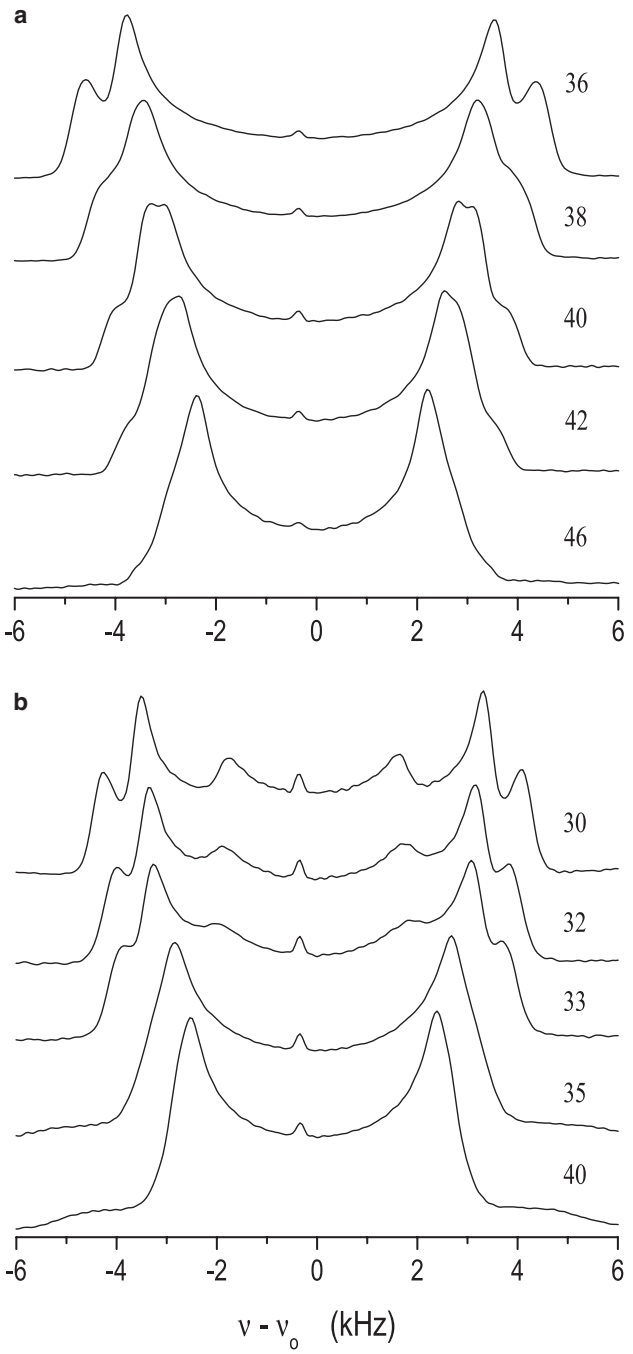

FIGURE 13 Variation of the methyl-group region of the ^{2}H NMR spectra with temperature (shown in °C in the figure) for two different sample DOPC/DPPC-d_{62}/cholesterol compositions with, molar proportions of (*a*) 0:75:25 and (*b*) 21:49:30. Both of these examples clearly show the effects of intermediate-timescale averaging at higher temperatures, and two-phase coexistence at temperatures >30°C.

widely known that T_{2e} varies strongly with position on the chain (from ~0.5 ms near the carbonyl group to nearly 2 ms for the methyl group) (66). Measurement of a single T_{2e} representing the chain positions in the order parameter plateau region, and using that single value to simulate a complex, multicomponent ^{2}H powder spectrum is an oversimplification. Of course, either fluctuations in local composition, as may occur near a critical composition, or intermediate-timescale exchange of DPPC-d_{62} molecules between regions with substantially different degrees of local order (such as domains of l_d and l_o phases), will lead to enhanced transverse relaxation, so such measurements are potentially very useful in defining the nature of the fluctuations occurring in these systems.

This phase diagram demonstrates that ternary mixtures of DOPC/DPPC-d_{62}/cholesterol exhibit a broad region of l_d-l_o two-phase coexistence both as a function of temperature and composition. The coexisting domains vary in size and relative proportion depending on temperature and composition. There is compelling evidence for fluctuations in the observed quadrupolar splittings arising either from exchange of molecules between domains or from fluctuations arising as a result of being close to a line of critical compositions.

To answer some of the questions raised in the analysis of the results presented here, which were obtained using chain perdeuterated DPPC-d_{62}, we are using specifically labeled DPPC. This will greatly simplify the interpretation of the spectra, especially at low temperatures (in the gel-phase region) and in situations where there is more than one phase. We are also trying to develop a more robust method of determining the endpoint compositions of both two- and three-phase coexistence regions. Further work that more precisely defines any phase boundaries present in both DOPC/cholesterol and DOPC/DPPC mixtures will be important to our efforts to refine the phase diagram.

We are most indebted to Frances J. Sharom for promoting an interest in the "raft" question. We thank M. Boudreau, M. Schmidt, and L. Ziani for their help in acquiring some of the spectra and for sharing their DOPC/DPPC-d_{62} data with us. We are also grateful for the technical assistance of Valerie Robertson.

This work was supported by grants from the Natural Sciences and Engineering Research Council of Canada, the Canada Foundation for Innovation, and the Ontario Research Fund.

REFERENCES

1. Simons, K., and E. Ikonen. 1997. Functional rafts in cell membranes. *Nature*. 387:569–572.
2. Brown, D. A., and E. London. 1997. Structure of detergent-resistant membrane domains: does phase separation occur in biological membranes? *Biochem. Biophys. Res. Commun*. 240:1–7.
3. London, E. 2005. How principles of domain formation in model membranes may explain ambiguities concerning lipid raft formation in cells. *Biochim. Biophys. Acta*. 1746:203–220.
4. Vist, M. R., and J. H. Davis. 1990. Phase equilibria of cholesterol/dipalmitoylphosphatidylcholine mixtures: ^{2}H nuclear magnetic resonance and differential scanning calorimetry. *Biochemistry*. 29:451–464.
5. Huang, T. -H., C. W. B. Lee, S. K. Das Gupta, A. Blume, and R. G. Griffin. 1993. A 13C and 2H nuclear magnetic resonance study of phosphatidylcholine/cholesterol interactions. characterization of liquid-gel phases. *Biochemistry*. 32:13277–13287.
6. Hsueh, Y. -W., K. T. Gilbert, C. Trandum, M. Zuckerman, and J. Thewalt. 2005. The effect of ergosterol on dipalmitoylphosphatidylcholine

bilayers: a deuterium NMR and calorimetric study. *Biophys. J.* 88:1799–1808.

7. Vist, M.R. 1984. Partial phase behavior of perdeuteriated dipalmitoylphosphatidylcholine-cholesterol model membranes. MSc thesis. University of Guelph, Guelph, Ontario, Canada.
8. Davis, J. H. 1986. NMR studies of cholesterol orientational order and dynamics, and the phase equilibria of cholesterol/phospholipid mixtures. *In* Physics of NMR Spectroscopy in Biology and Medicine. B. Maraviglia, editor. North Holland, Amsterdam, pp. 302–312.
9. Oldfield, E., and D. Chapman. 1971. Effects of cholesterol and cholesterol derivatives on hydrocarbon chain mobility in lipids. *Biochem. Biophys. Res. Commun.* 43:610–616.
10. Oldfield, E., M. Meadows, D. Rice, and R. Jacobs. 1978. Spectroscopic studies of specifically deuterium labeled membrane systems. Nuclear magnetic resonance investigation of the effects of cholesterol in model systems. *Biochemistry.* 17:2727–2740.
11. Davis, J. H., M. Bloom, K. W. Butler, and I. C. P. Smith. 1980. The temperature dependence of molecular order and the influence of cholesterol in *Acholeplasma Laidlawii* membranes. *Biochim. Biophys. Acta.* 597:477–491.
12. Davis, J. H. 1993. The molecular dynamics, orientational order, and thermodynamic phase equilibria of cholesterol/phosphatidylcholine mixtures: ^{2}H nuclear magnetic resonance. *In* Cholesterol in Membrane Models. L. Finegold, editor. CRC Press, Boca Raton, FL, pp. 67–135.
13. Chachaty, C., D. Rainteau, C. Tessier, P. J. Quinn, and C. Wolf. 2005. Building up of the liquid-ordered phase formed by sphingomyelin and cholesterol. *Biophys. J.* 88:4032–4044.
14. Maraviglia, B., J. H. Davis, M. Bloom, J. Westerman, and K. W. A. Wirtz. 1982. Human erythrocytes are fluid down to −5°C. *Biochim. Biophys. Acta.* 686:137–140.
15. Needham, D., T. J. McIntosh, and E. Evans. 1988. Thermomechanical and transition properties of dimyristoylphosphatidylcholine/cholesterol bilayers. *Biochemistry.* 27:4668–4673.
16. Needham, D., and R. S. Nunn. 1990. Elastic deformation and failure of lipid bilayer membranes containing cholesterol. *Biophys. J.* 58:997–1009.
17. Rubenstein, J. L., B. A. Smith, and H. M. McConnell. 1979. Lateral diffusion in binary mixtures of cholesterol and phosphatidylcholines. *Proc. Natl. Acad. Sci. USA.* 76:15–18.
18. Weisz, K., G. Grobner, C. Mayer, J. Stohrer, and G. Kothe. 1992. Deuteron nuclear magnetic resonance study of the dynamic organization of phospholipid/cholesterol bilayer membranes: molecular properties and viscoelastic behavior. *Biochemistry.* 31:1100–1112.
19. Lindblom, G., and G. Orrad. 1994. NMR studies of translational diffusion in lyotropic liquid-crystals and lipid-membranes. *Prog. NMR Spectrosc.* 26:483–515.
20. Filippov, A., G. Oradd, and G. Lindblom. 2003. The effect of cholesterol on the lateral diffusion of phospholipids in oriented bilayers. *Biophys. J.* 84:3079–3086.
21. Gaede, H. C., and K. Gawrisch. 2003. Lateral diffusion rates of lipid, water, and a hydrophobic drug in a multilamellar liposome. *Biophys. J.* 85:1734–1740.
22. Holland, G. P., S. K. McIntyre, and T. M. Alam. 2006. Distinguishing individual lipid headgroup mobility and phase transitions in raft-forming lipid mixtures with ^{31}P MAS NMR. *Biophys. J.* 90:4248–4260.
23. Ipsen, J. H., G. Karlstrom, O. G. Mouritsen, H. Wennerstrom, and M. J. Zuckermann. 1987. Phase equilibria in the phosphatidylcholine-cholesterol system. *Biochim. Biophys. Acta.* 905:162–172.
24. Veatch, S. L. 2007. From small fluctuations to large-scale phase separation: lateral organization in model membranes containing cholesterol. *Semin. Cell Dev. Biol.* 18:573–582.
25. Veatch, S. L., O. Soubias, S. L. Keller, and K. Gawrisch. 2007. Critical fluctuations in domain-forming lipid mixtures. *Proc. Natl. Acad. Sci. USA.* 104:17650–17655.
26. Dietrich, C., L. A. Bagatolli, Z. N. Volovyk, N. L. Thompson, M. Levi, et al. 2001. Lipid rafts reconstituted in model membranes. *Biophys. J.* 80:1417–1428.
27. Feigenson, G. W., and J. T. Buboltz. 2001. Ternary phase diagram of dipalmitoyl-PC/dilauroyl-PC/cholesterol: nanoscopic domain formation driven by cholesterol. *Biophys. J.* 80:2775–2788.
28. Baumgart, T., S. T. Hess, and W. W. Webb. 2003. Imaging coexisting fluid domains in biomembrane models coupling curvature and line tension. *Nature.* 425:821–824.
29. de Almeida, R. F. M., A. Fedorov, and M. Prieto. 2003. Sphingomyelin/phosphatidylcholine/cholesterol phase diagram: boundaries and composition of lipid rafts. *Biophys. J.* 85:2406–2416.
30. Scherfeld, D., N. Kahya, and P. Schwille. 2003. Lipid dynamics and domain formation in model membranes composed of ternary mixtures of unsaturated and saturated phosphatidylcholines and cholesterol. *Biophys. J.* 85:3758–3768.
31. Veatch, S. L., and S. L. Keller. 2003. Separation of liquid phases in giant vesicles of ternary mixtures of phospholipids and cholesterol. *Biophys. J.* 85:3074–3083.
32. Simons, K., and W. L. C. Vaz. 2004. Model systems, lipid rafts, and cell membranes. *Annu. Rev. Biophys. Biomol. Struct.* 33:269–295.
33. Veatch, S. L., I. V. Polozov, K. Gawrisch, and S. L. Keller. 2004. Liquid domains in vesicles investigated by NMR and fluorescence microscopy. *Biophys. J.* 86:2910–2922.
34. Heberle, F. A., J. T. Buboltz, D. Stringer, and G. W. Feigenson. 2005. Fluorescence methods to detect phase boundaries in lipid bilayer mixtures. *Biochim. Biophys. Acta.* 1746:186–192.
35. Veatch, S. L., and S. L. Keller. 2005. Seeing spots: complex phase behavior in simple membranes. *Biochim. Biophys. Acta.* 1746:172–185.
36. Veatch, S. L., and S. L. Keller. 2005. Miscibility phase diagrams of giant vesicles containing sphingomyelin. *Phys. Rev. Lett.* 94:148101.
37. Veatch, S. L., K. Gawrisch, and S. L. Keller. 2006. Closed-loop miscibility gap and quantitative tie-lines in ternary membranes containing diphytanoyl PC. *Biophys. J.* 90:4428–4436.
38. Bagatolli, L. A. 2006. To see or not to see: lateral organization of biological membranes and fluorescence microscopy. *Biochim. Biophys. Acta.* 1758:1541–1556.
39. Coste, V., N. Puff, D. Lockau, P. J. Quinn, and M. I. Angelova. 2006. Raft-like domain formation in large unilamellar vesicles probed by the fluorescent phospholipid analogue, C_{12}NBD-PC. *Biochim. Biophys. Acta.* 1758:460–467.
40. Veatch, S. L., S. S. W. Leung, R. E. W. Hancock, and J. L. Thewalt. 2007. Fluorescent probes alter miscibility phase boundaries in ternary vesicles. *J. Phys. Chem. B.* 111:502–504.
41. Aussenac, F., M. Tavares, and E. J. Dufourc. 2003. Cholesterol dynamics in membranes of raft composition: a molecular point of view from 2H and 31P solid-state NMR. *Biochemistry.* 42:1383–1390.
42. Clarke, J. A., A. J. Heron, J. M. Seddon, and R. V. Law. 2006. The diversity of the liquid ordered (L_o) phase of phosphatidylcholine/cholesterol membranes: a variable temperature multinuclear solid-state NMR and x-ray diffraction study. *Biophys. J.* 90:2383–2393.
43. Lindblom, G., and G. Orrad. 2007. Order and disorder in a liquid crystalline bilayer: pulsed field gradient NMR studies of lateral phase separation. *J. Disper. Sci. Technol.* 28:55–61.
44. Samsonov, A. V., I. Mihalyov, and F. S. Cohen. 2001. Characterization of cholesterol-sphingomyelin domains and their dynamics in bilayer membranes. *Biophys. J.* 81:1486–1500.
45. Tokumasu, F., A. J. Jin, G. W. Feigenson, and J. A. Dvorak. 2003. Atomic force microscopy of nanometric liposome adsorption and nanoscopic membrane domain formation. *Ultramicroscopy.* 97:217–227.
46. Zuckermann, M. J., J. H. Ipsen, L. Miao, O. G. Mouritsen, M. Nielsen, et al. 2004. Modeling lipid-sterol bilayers: applications to structural evolution, lateral diffusion, and rafts. *Methods Enzymol.* 383: 198–229.
47. de Almeida, R. F. M., L. M. S. Loura, A. Fedorov, and M. Prieto. 2005. Lipid rafts have different sizes depending on membrane composition: a time-resolved fluorescence resonance energy transfer study. *J. Mol. Biol.* 346:1109–1120.

48. Chiang, Y. -W., J. Zhao, J. Wu, Y. Shimoyama, J. H. Freed, et al. 2005. New method for determining tie-lines in coexisting membrane phases using spin-label ESR. *Biochim. Biophys. Acta.* 1668:99–105.
49. Elliott, R., K. Katsov, M. Schick, and I. Szleifer. 2005. Phase separation of saturated and mono-unsaturated lipids as determined from a microscopic model. *J. Chem. Phys.* 122:044904(1)–044904(11).
50. Pencer, J., T. Mills, V. Anghel, S. Krueger, R. M. Epand, et al. 2005. Detection of submicron-sized raft-like domains in membranes by small-angle neutron scattering. *Eur. Phys. J. E. Soft Matter.* 18:447–458.
51. Aittoniemi, J., P. S. Niemela, M. T. Hyvonen, M. Karttunen, and I. Vattulainen. 2007. Insight into the putative specific interactions between cholesterol, sphingomyelin, and palmitoyl-oleoyl phosphatidylcholine. *Biophys. J.* 92:1125–1137.
52. de Almeida, R. F. M., J. W. Borst, A. Fedorov, M. Prieto, and A. J. W. G. Visser. 2007. Complexity of lipid domains and rafts in giant unilamellar vesicles revealed by combining imaging, microscopic and macroscopic time-resolved fluorescence. *Biophys. J.* 93:539–553.
53. Frazier, M. L., J. R. Wright, A. Pokorny, and P. F. F. Almeida. 2007. Investigation of domain formation in sphingomyelin/cholesterol/POPC mixtures by fluorescence resonance energy transfer and Monte Carlo simulations. *Biophys. J.* 92:2422–2433.
54. Lin, W. -C., C. D. Blanchette, and M. L. Longo. 2007. Fluid-phase chain unsaturation controlling domain microstructure and phase in ternary lipid bilayers containing GalCer and cholesterol. *Biophys. J.* 92:2831–2841.
55. Davis, J. H. 1979. Deuterium magnetic resonance study of the gel and liquid crystalline phases of dipalmitoyl phosphatidylcholine. *Biophys. J.* 27:339–358.
56. Huschilt, J. C., R. S. Hodges, and J. H. Davis. 1985. Phase equilibria in an amphiphilic peptide-phospholipid model membrane by deuterium nuclear magnetic resonance difference spectroscopy. *Biochemistry.* 24:1377–1386.
57. Gupta, C. M., R. Radhakrishnan, and H. G. Khorana. 1977. Glycerophospholipid synthesis: improved general method and new analogs containing photoactivable groups. *Proc. Natl. Acad. Sci. USA.* 74:4315–4319.
58. Buboltz, J. T., and G. W. Feigenson. 1999. A novel strategy for the preparation of liposomes: rapid solvent exchange. *Biochim. Biophys. Acta.* 1417:232–245.
59. Huang, J., J. T. Buboltz, and G. W. Feigenson. 1999. Maximum solubility of cholesterol in phosphatidylcholine and phosphatidylethanolamine bilayers. *Biochim. Biophys. Acta.* 1417:89–105.
60. Muhr, P., W. Likussar, and M. Schubert-Zsilavecz. 1996. Structure investigation and proton and carbon-13 assignments of digitonin and cholesterol using multidimensional NMR techniques. *Magn. Reson. Chem.* 34:137–142.
61. Seelig, J., F. Borle, and T. A. Cross. 1985. Magnetic ordering of phospholipid membranes. *Biochim. Biophys. Acta.* 814:195–198.
62. Speyer, J. B., P. K. Sripada, S. K. D. Gupta, G. G. Shipley, and R. G. Griffin. 1987. Magnetic orientation of sphingomyelin-lecithin bilayers. *Biophys. J.* 51:687–691.
63. Davis, J. H., K. R. Jeffrey, M. Bloom, M. I. Valic, and T. P. Higgs. 1976. Quadrupolar echo deuteron magnetic resonance spectroscopy in ordered hydrocarbon chains. *Chem. Phys. Lett.* 42:390–394.
64. Bloom, M., J. H. Davis, and M. I. Valic. 1980. Spectral distortion effects due to finite pulse widths in deuterium nuclear magnetic resonance spectroscopy. *Can. J. Phys.* 58:1510–1517.
65. Hoult, D. I., and R. E. Richards. 1975. Critical factors in the design of sensitive high resolution nuclear magnetic resonance spectrometers. *Proc. R. Soc. Lond. A.* 344:311–340.
66. Davis, J. H. 1983. The description of membrane lipid conformation, order and dynamics by ^{2}H-NMR. *Biochim. Biophys. Acta.* 737:117–171.
67. Prosser, R. S., J. H. Davis, F. W. Dahlquist, and M. A. Lindorfer. 1991. 2H nuclear magnetic resonance of the gramicidin A backbone in a phospholipid bilayer. *Biochemistry.* 30:4687–4696.
68. Masing, G. 1944. Ternary Systems: Introduction to the Theory of Three Component Systems. Dover Publications, New York.
69. Bienvenue, A., M. Bloom, J. H. Davis, and P. F. Devaux. 1982. Evidence for protein-associated lipids from deuterium nuclear magnetic resonance studies of rhodopsin-dimyristoylphosphatidylcholine recombinants. *J. Biol. Chem.* 257:3032–3038.
70. Schindler, H. -G., and J. Seelig. 1975. Deuterium order parameters in relation to thermodynamic properties of a phospholipid bilayer. A statistical mechanical interpretation. *Biochemistry.* 14:2283–2287.
71. Davis, J. H., and K. R. Jeffrey. 1977. The temperature dependence of chain disorder in potassium palmitate-water. A deuterium NMR study. *Chem. Phys. Lipids.* 20:87–104.
72. Lange, A., D. Marsh, K. H. Wassmer, P. Meier, and G. Kothe. 1985. Electron spin resonance study of phospholipid membranes employing a comprehensive line-shape model. *Biochemistry.* 24:4383–4392.
73. Prosser, R. S., J. H. Davis, C. Mayer, K. Weisz, and G. Kothe. 1992. Deuterium NMR relaxation studies of peptide-lipid interactions. *Biochemistry.* 31:9355–9363.
74. Tardieu, A., V. Luzzati, and F. C. Reman. 1973. Structure and polymorphism of the hydrocarbon chains of lipids: a study of lecithin-water phases. *J. Mol. Biol.* 75:711–733.
75. Trouard, T. P., A. A. Nevzorov, T. M. Alam, C. Job, J. Zajicek, et al. 1999. Influence of cholesterol on dynamics of dimyristoylphosphatidylcholine bilayers as studied by deuterium NMR relaxation. *J. Chem. Phys.* 110:8802–8818.
76. Karmakar, S., and V. A. Raghunathan. 2005. Structure of phospholipid-cholesterol membranes: an x-ray diffraction study. *Phys. Rev. E Stat. Nonlin. Soft Matter Phys.* 71:061924.
77. Blume, A., R. J. Wittebort, S. K. Das Gupta, and R. G. Griffin. 1982. Phase equilibria, molecular conformation, and dynamics in phosphatidylcholine/phosphatidylethanolamine bilayers. *Biochemistry.* 21:6243–6253.
78. Ruocco, M. J., and G. G. Shipley. 1982. Characterization of the subtransition of hydrated dipalmitoylphosphatidylcholine bilayers. X-ray diffraction study. *Biochim. Biophys. Acta.* 684:59–66.
79. Tenchov, B., R. Koynova, and G. Rapp. 2001. New ordered metastable phases between the gel and subgel phases in hydrated phospholipids. *Biophys. J.* 80:1873–1890.
80. Lindblom, G., G. Orrad, and A. Filippov. 2006. Lipid lateral diffusion in bilayers with phosphatidylcholine, sphingomyelin and cholesterol. An NMR study of dynamics and lateral phase separation. *Chem. Phys. Lip.* 141:179–184.
81. Lentz, B. R., Y. Barenholz, and T. E. Thompson. 1976. Fluorescence depolarization studies of phase transitions and fluidity in phospholipid bilayers. 2. Two-component phosphatidylcholine liposomes. *Biochemistry.* 15:4529–4537.
82. Davis, P. J., and K. M. W. Keough. 1983. Differential scanning calorimetric studies of aqueous dispersions of mixtures of cholesterol with some mixed-acid and single-acid phosphatidylcholines. *Biochemistry.* 22:6334–6340.
83. Ipsen, J. H., and O. G. Mouritsen. 1988. Modelling the phase equilibria in two-component membranes of phospholipids with different acyl-chain lengths. *Biochim. Biophys. Acta.* 944:121–134.
84. Ipsen, J. H., K. Jorgensen, and O. G. Mouritsen. 1990. Density fluctuations in saturated phospholipid bilayers increase as the acyl-chain length decreases. *Biophys. J.* 58:1099–1107.
85. Harries, D., and A. Ben-Shaul. 1997. Conformational chain statistics in a model lipid bilayer: comparison between mean field and Monte Carlo calculations. *J. Chem. Phys.* 106:1609–1619.
86. Mukhin, S. I., and S. Baoukina. 2005. Analytical derivation of thermodynamic characteristics of lipid bilayer from a flexible string model. *Phys. Rev. E Stat. Nonlin. Soft Matter Phys.* 71:0161918.
87. Scheldt, H. A., D. Huster, and K. Gawrisch. 2005. Diffusion of cholesterol and its precursors in lipid membranes studied by ^{1}H pulsed field gradient magic angle spinning NMR. *Biophys. J.* 89:2504–2512.
88. Brown, M. F., and J. H. Davis. 1981. Orientation and frequency dependence of the deuterium spin-lattice relaxation in multilamellar phospholipid dispersions: implications for dynamic models of membrane structure. *Chem. Phys. Lett.* 79:431–435.